POLITECNICO DI TORINO

Department of Environment, Land and Infrastructure Engineering

Master of Science
in Petroleum and Mining Engineering

Diffusion phenomena analysis for CO_2 storage purposes

Supervisor
Prof. Francesca Verga

.....

Co-supervisor
Prof. Dario Viberti

.....

Co-supervisor
Prof. Marzia Quaglio

.....

Student
Elnur Garashov

.....

A.A.19/20

Context

1 Introduction

The Earth's climate is increasingly altering by human activities. One of the concerns is related to the concentration of greenhouse gas in the atmosphere. The most significant greenhouse gas is CO_2. Consequently, the amount of CO_2 must be decreased. This can be accomplished by means of carbon dioxide capture and storage (CCS), also known as CO_2 sequestration.

The entrapment of CO_2 in the oil reservoirs during CO_2-based EOR has recently started to be considered to use in conjunction. It is a win-win project in which the recovery factor can be increased, while the amount of greenhouse gas emissions-reduced. The costs of CO_2 capture and storage can, in many cases, be compensated by improved recovery.

To ensure long-term secure storage, it is necessary to take into account a number of possibilities of failure of CO_2 sequestration, such as diffusion of CO_2 through seal rock, loss of the seal rock integrity, etc. The diffusion phenomena analysis for CO_2 storage purposes was the scope of this study.

The current thesis presents a critical review of technical literature dedicated to the description of the diffusion phenomena, the introduction of different diffusion coefficient measurement methodologies, characterization of diffusion coefficients through laboratory experiments. Furthermore, a number of diffusion coefficients provided by literature are reported and analyzed.

2 State of art

2.1 CO_2 Injection in Geological Formation

The injections of CO_2 into the geological formations are accomplished for enhanced oil recovery (EOR), enhanced gas recovery (EGR), storage and sequestration of anthropogenic greenhouse gas emissions [1]. Phenomena involved in any CO_2 injection into the geological formations are the following:

- Convection
- Dispersion or mixing
- Chemical reactions
- Geomechanical effects

The key objective of employment EOR and EGR is to increase hydrocarbons production from oil and gas reservoirs. In case of purely storage options, the injection of CO_2 is performed without direct benefits from an economic point of view, e.g. saline aquifers. The economic viability of this option can be improved by tax credits of carbon [1]. Aquifers that don't contain potable water are defined as saline aquifers. The ability of saline aquifers to store the total CO_2 emissions in different locations near the sources of the CO_2 emissions, such as power plants, is huge.

The efficiency of CO_2 utilization processes is based on the increment of hydrocarbon recovery, final hydrocarbon recovery and CO_2 recovery which can be used for recycling purposes. It is worth highlighting that the main expense of the CO_2 injection is the purchase of CO_2 [2].

CO_2 entrapment in the oil reservoirs during EOR by CO_2 has recently started to be used in conjunction in order to control the greenhouse gas emission. It is a win-win project in which we are able to improve the recovery factor as well as decrease the amount of greenhouse gas emissions [3]. In the case of EOR, the injection of CO_2 into the oil reservoirs is performed at pressures higher or close to minimum

miscibility pressure (MMP). The reason for this is at pressures above MMP the oil and injected CO_2 mixes duly and the composition's behavior is close to single-phase flow. As soon as the injection has been performed, CO_2 mixes with the oil in the interstitial spaces. This process is mainly governed by molecular diffusion and convective mixing. Due to pressure forces or convection, the propagation of the injected CO_2 plume occurs. While propagation and mixing take place, the fraction of CO_2 molecules contacts with the connate water. As soon as contact with brine occurs, CO_2 dissolves in the connate water and start reactions [1]. During the dissolution of CO_2 in the brine the following reactions originate readily:

$$H_2O + CO_2 \leftrightarrow H_2CO_3 \quad (1)$$

$$H_2CO_3 \leftrightarrow H^+ + HCO_3^- \quad (2)$$

$$HCO_3^- \leftrightarrow H^+ + CO_3^{2-} \quad (3)$$

The bicarbonate which has been dissolved reacts with divalent cations to dissolve in or precipitate on carbonate minerals. These latter reactions are slower in comparison with the former ones.

$$HCO_3^- + Ca^{2+} \leftrightarrow CaCO_3 + H^+ \quad (4)$$

$$HCO_3^- + Mg^{2+} \leftrightarrow MgCO_3 + H^+ \quad (5)$$

$$HCO_3^- + Fe^{2+} \leftrightarrow FeCO_3 + H^+ \quad (6)$$

In case of the injection of CO_2 into saline aquifers, there are no hydrocarbons in the system and the propagation process of CO_2 into the formation is governed by dispersion and convection. Dispersion is triggered by convective mixing and molecular diffusion. In the early stages of the injection process, the convection mixing takes place mainly due to the velocity field linked to the pressure gradient and slightly by reason of the viscosity and density differences between supercritical CO_2 and brine. In the event of good vertical conductivity, on account

of CO_2/brine density contrast, the injected CO_2 tends to flow in an upward direction. The flow in an upward direction proceeds until it reaches the caprock. As soon as CO_2 is captured by the seal rock it interacts with brine which is located underneath and forms slights denser fluid which tends to flow downward. This flow in a downward direction occurs owing to the gravity effect. An unstable diffusive boundary layer has been induced by this gravity effect which eventually facilitates convective mixing. This process takes place extremely slow. The reason for that is the density difference between brine in contact with CO_2 and virgin brine is very small. Even though this process is very slow, it might be effective in the long-term CO_2 sequestration process [4].

2.2 Underground CO_2 Storage

The Earth's climate is increasingly altering by human activities. One of the concerns is related to the concentration of CO_2 in the atmosphere. Its amount may rise fast as a consequence of the growth of industrialization [8].

The most significant greenhouse gas is CO_2. The permanent accumulation of greenhouse gas in the atmosphere from different anthropogenic sources is believed to be the primary reason for the temperature increase of the Earth's surface [9,10]. The sources of the largest anthropogenic CO_2 emissions are electricity generation and stationery industry sectors powered by fossil fuels [11].

The production of CO_2 from fossil fuels is not expected to slow down soon. In view of the circumstances, it is required to find somewhere besides the atmosphere to place the increased concentrations of CO_2.

2.2.1 Sequestration

Carbon dioxide capture and storage (CCS), which is also known as CO_2 sequestration, is a technology that can capture the carbon dioxide (CO_2) emissions produced from the use of fossil fuels, preventing carbon dioxide from entering the atmosphere.

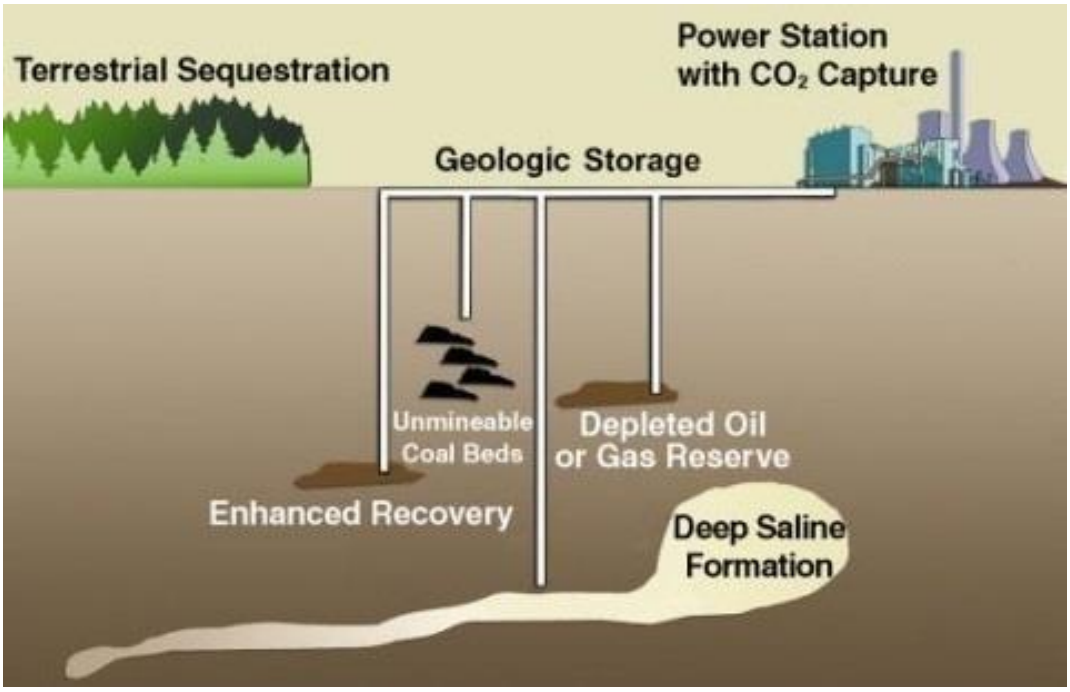

Figure 2-1. Carbon dioxide sequestration options [12]

Several possibilities are sequestration in the ocean, soils, and forests. An additional option is sequestration in geological formations which may also become an important solution. Depleted oil and gas reservoirs, unsuitable for industrial development coal seams and deep saline aquifers are examples of such formations. The costs of CO_2 entrapment and sequestration, in many cases, can be compensated by means of enhanced recovery.

The chain of Carbon dioxide Capture and Storage consists of three parts; capturing the carbon dioxide, transporting the carbon dioxide, and securely storing the carbon dioxide emissions underground.

First, the capture of carbon dioxide can be done by three methods: pre-combustion capture, post-combustion capture, and oxy-fuel combustion. The further step consists of carbon dioxide transportation by pipeline or ship for safe storage. Millions of tons of carbon dioxide are already transported annually for commercial purposes by road tankers, ships, and pipelines. Further, CO_2 is carefully stored in the selected appropriate geological rock formation. These geological rock formations are mainly located a few kilometers from the surface.

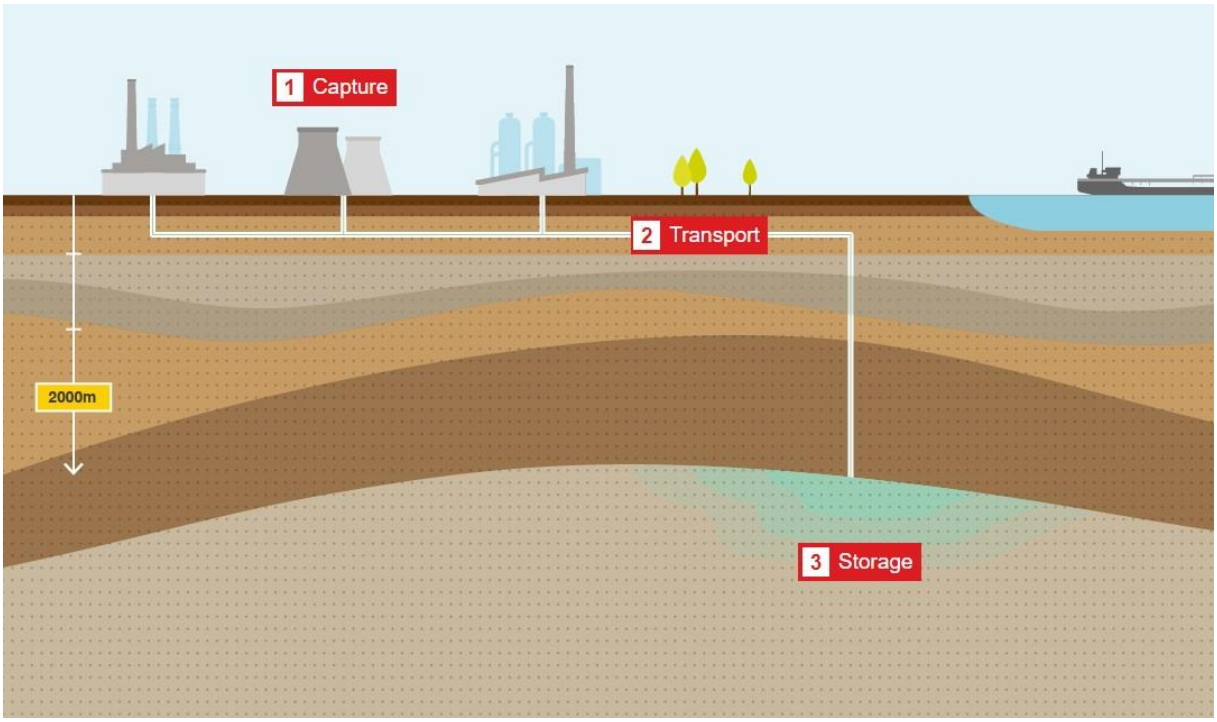

Figure 2-2. Carbon dioxide capture and storage chain [13]

Despite the fact that the geological sequestration of CO_2 is feasible, further studies are required to implement this method in the most efficient way. First of all, identification of sequestration sites and assessment of the geological formations capacities must be performed. Additionally, due to the fact that the main objective of all is the insurance of the safe storage of CO_2, the monitoring technologies must be developed in order to assure the public. Nowadays, scientists are concerned with the investigation of the ways to improve the capturing technologies of CO_2 which will have a positive effect on the overall cost of geological sequestration [8].

The majority of CO_2 capture and storage literature has focused on the assessments of the storage potential of deep saline formations, due to their distinctive accumulation potentials, and oil reservoirs for EOR [14,15]. Depleted gas reservoirs for storage purposes are smaller in comparison with former ones. However, they can be characterized by the following advantages:

- Easier target because of known capacity
- Rock characterization

- Proven containment
- Existing surface facilities that can be used for CO_2 storage

The CO_2 storage capacity of depleted gas reservoirs all over the world is estimated to be approximately 390 gigatons, which is based on a void replacement ratio of 60% of reservoirs [16]. This value of storage ability represents ten times the current annual CO_2 emissions worldwide and could be also a usable decision for CO_2 sequestration. Nevertheless, the main challenges encountered by the field development are CO_2 capture and transportation.

The most efficient state of CO_2 storage in underground formations is supercritical than the gaseous or liquid state. As a consequence, the employment of shallow reservoirs is not appropriate for CO_2 sequestration due to the fact that CO_2 will be in gaseous or liquid state [17,18]. Increased storage and entrapment are expected in reservoirs deeper than 800 m (2600 ft). Under these circumstances, the temperature and pressure are favorable to provide the supercritical state of CO_2. The transition to supercritical state occurs at Tc = 88°F (31.1°C) and Pc = 1070 psia (73.8 bar).

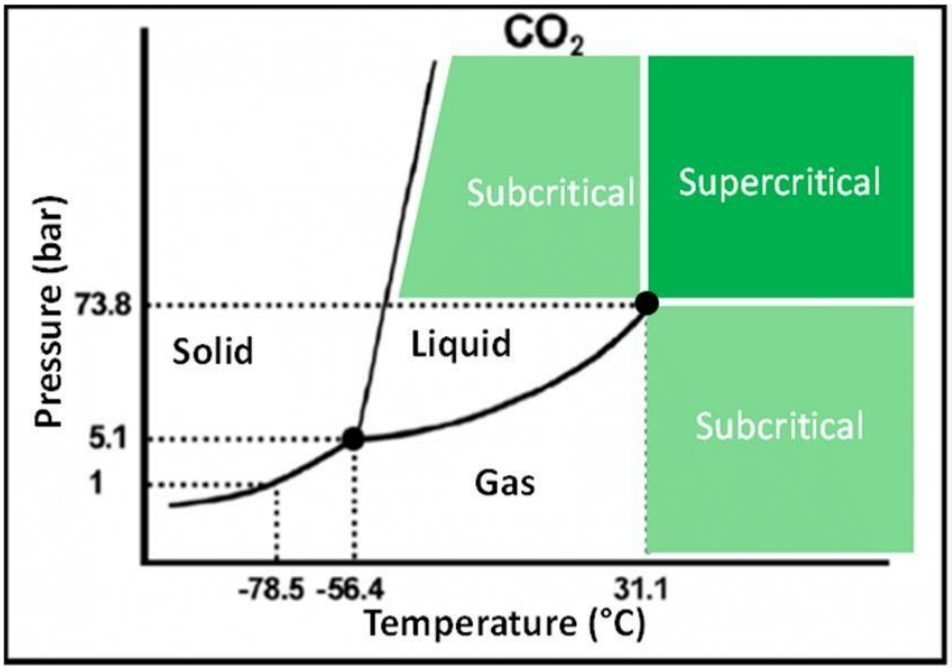

Figure 2-3. Phase diagram of CO_2

2.2.2 Issues of CO_2 sequestration

Typical technical challenges that can be encountered during CO_2 sequestration are the following:

- Drilling complications in depleted zones
- Well integrity
- Transport
- Monitoring
- Capture
- Dehydration
- Compression

During the transition of CO_2 from the denser state to the gas state exerts temperature cooling, flow velocity acceleration and pressure chokes which can negatively affect CO_2 injectivity, wellhead control, and wellbore integrity.

Early during the injection process, the injected CO_2 will vaporize, while the pressure in the reservoir builds up to the bubble point of CO_2. The flashpoint of CO_2 will be achieved between the subsurface reservoir and the wellhead. This can lead to several scenarios [5]:

Scenario 1- CO_2 vaporization inside of the well tubing: In case, if the vaporization of CO_2 takes place within the well tubing in which there is the presence of water, it can result in the formation of hydrates inside of it [19]. The formation of hydrates is directly associated with the presence of water, which means that if the water is absent no hydrates will form. Nevertheless, the risk of hydrate formation as a result of the vaporization process inside the well tubing will remain relevant in the reservoir because of the fact that cooled gaseous CO_2 will reach wet sand near the wellbore.

Scenario 2—CO_2 vaporization across the perforations: The worth scenario might be the vaporization of CO_2 across the perforations or within a few feet of the wellbore. In an account of more localized cooling, there is a possibility of a

generation not only hydrates but also dry ice across the zone of perforation. It results in the loss of injectivity.

Scenario 3—CO_2 vaporization within the reservoir: The vaporization of CO_2 inside of the reservoir is less problematic if it happens away from the wellbore since the complete plugging is not expected to occur. It can cause a partial loss of injectivity.

2.3 Enhanced Oil Recovery

Oil reservoirs development and production can be divided into three phases:

- Primary recovery
- Secondary recovery
- Tertiary (or enhanced) recovery

Primary recovery is associated with the undertaking of oil up to the surface by means of the natural energy of the reservoir which may involve techniques for artificial lift (e.g. pumps) [20]. This method provides a recovery factor of approximately 20% of total oil originally in place (OOIP). Further extension of a field's production life can be achieved by injecting water or gas in order to displace oil to a production well. This results in a recovery of 20% to 60% of the OOIP. Using these two methods, the most part of the reservoir remains unproduced. Enhanced oil recovery (EOR) improves the amount of oil recovered up to 50 to 80 percent, or even more, of OOIP [20]. Regardless of the fact that it has been performed either after primary and secondary recovery or at an early stage of production, it enhances the oil displacement in the reservoir and restores formation pressure.

2.3.1 Definition

Enhanced Oil Recovery is defined as the operation which performs to increment the amount of recoverable oil from an oil reservoir. This is done by injecting a

substance into an oil well with an aim to reduce the viscosity of the oil, which is one of the important parameters in the extraction process, and increase the pressure. This leads to an increase in oil recovery by up to 15% [21].

The following major categories of EOR can be highlighted:

- Gas injection
- Thermal injection
- Chemical injection
- CO_2 injection

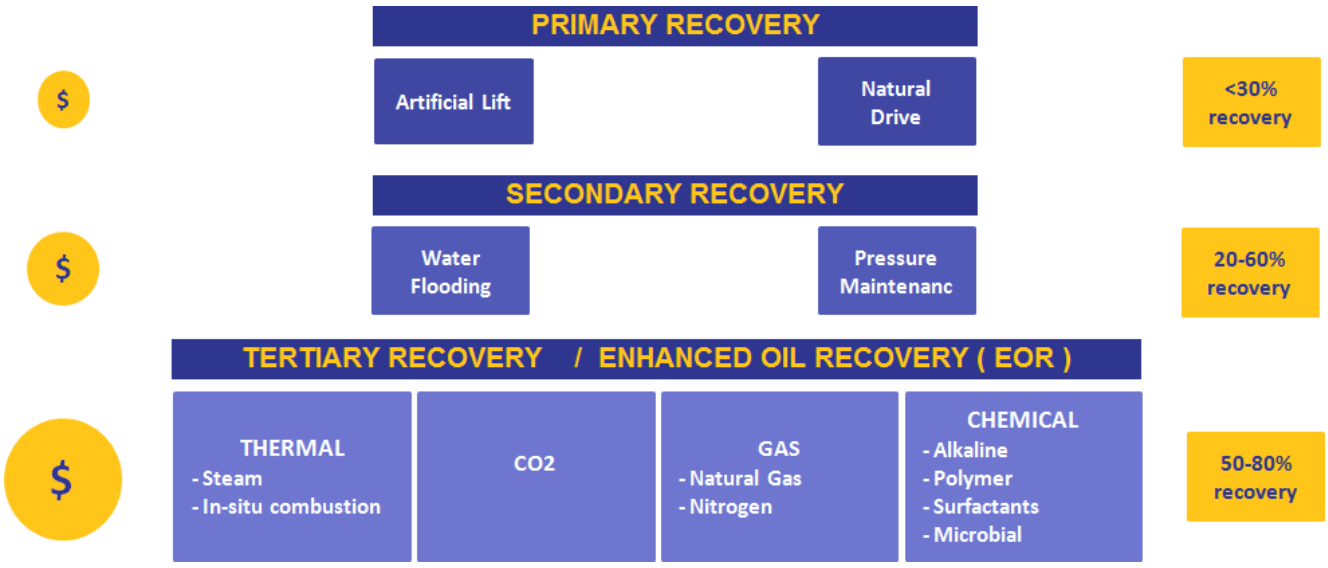

Figure 2-4. Reservoirs development and production phases [22]

Difficulties in using EOR methods are associated with the high cost and, in some cases, by the unpredictability of its effectiveness.

It is worthwhile to emphasize that due to the increment of development cost in conjunction with hydrocarbons production, EOR techniques are not employed on all wells and reservoirs. It must make sense from the economic point of view. As a consequence, once it has been decided to use EOR, it needs to be carefully analyzed to select the most appropriate and efficient methodology. This can be

performed by means of characterization of the reservoir, screening, scoping, reservoir modeling and simulation [23].

The main factors which affect the optimal application of each type are reservoir temperature, pressure, permeability, porosity, net pay, residual oil, and connate water saturations and fluid properties such as viscosity and oil API gravity [24].

2.3.2 Gas Injection

The basic principle of gas injection is the usage of different gases to drive the oil to the surface and to lower its viscosity. The reduction of viscosity has a positive effect on the flow of oil. Natural gas, carbon dioxide, and nitrogen are used as an injected gas. However, the most popular EOR technique is the injection of CO_2. This method is gaining popularity more and more. Nowadays, CO_2 injection is used in about half of the EOR [23]. Initially, the utilization of CO_2 was limited by the fact that it could be applied near naturally occurring CO_2 reservoirs or the ones that located within the pipeline range. Now, the improvement of techniques makes CO_2 to be recycled from industrial applications (e.g. natural gas processing, fertilizer, ethanol, and hydrogen plants) in cases when the naturally occurring CO_2 reservoirs are not available. The US Department of Energy considers CO_2 injection for EOR as the most promising technique [23].

2.3.3 Thermal Injection

The thermal injection is used to liquefy the oil by heat to smooth the extraction process. Steam flooding and fire flooding are examples of thermal injection methodology. In the case of steam flooding, the stem is pushed into the well which condenses into hot water and results in the heated oil with reduced viscosity. Fire flooding based on the injection of oxygen with the purpose of oil combustion on the circumference of the reservoir. This process produces enough warmth to move oil close to the well [25].

2.3.4 Chemical Injection

The chemical injection includes injection of long-chained molecules called polymers or detergent-like surfactants. The role of polymers is to improve the water flooding process which is done by reduction of oil viscosity, whereas surfactants affect the surface tension, so as to reduce it, which precludes the movement of oil throughout a reservoir. CO_2 flooding in a liquid state in very deep wells leads to swelling of oil and an increase of pressure [26].

2.3.5 CO_2 Injection

The principle of CO_2 injection is to behave as a solvent, a pressurizing agent and reduce the viscosity of the oil. The reasons for CO_2 injection for being a good option in comparison with other techniques are the following [27]:

- Miscible with crude oil
- Less expensive than other miscible fluid with similar properties

In addition to enhancing the recovery, the main advantage of CO_2 injection is the usage of it. Due to its popularity in EOR, the technologies for capturing it to remove greenhouse gas is improving day by day. As a consequence, EOR is a catalyzer for a carbon market [21].

In the case of the application of CO_2 the oil recovery increases by means of a viscous fluid drive, oil phase swelling and oil viscosity reduction. The reason for achieving a high recovery factor is also associated with miscibility, which reduces the interfacial tension between oil and gas and diminishes the capillary differences between fractures and matrix.

As soon as CO_2 has been injected in a crude oil/brine/rock system, multi-contact miscibility develops as a result of several exchange processes. This happens if the injection pressure for a given temperate exceeds the minimum miscibility pressure (MMP). Further, through the vaporization process, hydrocarbon components fall

into the CO_2, while CO_2 condensate into the oil phase. This process proceeds until it can be considered as one phase. During this process, the vaporization of light components into the gas phase occurs easier than heavy ones [27].

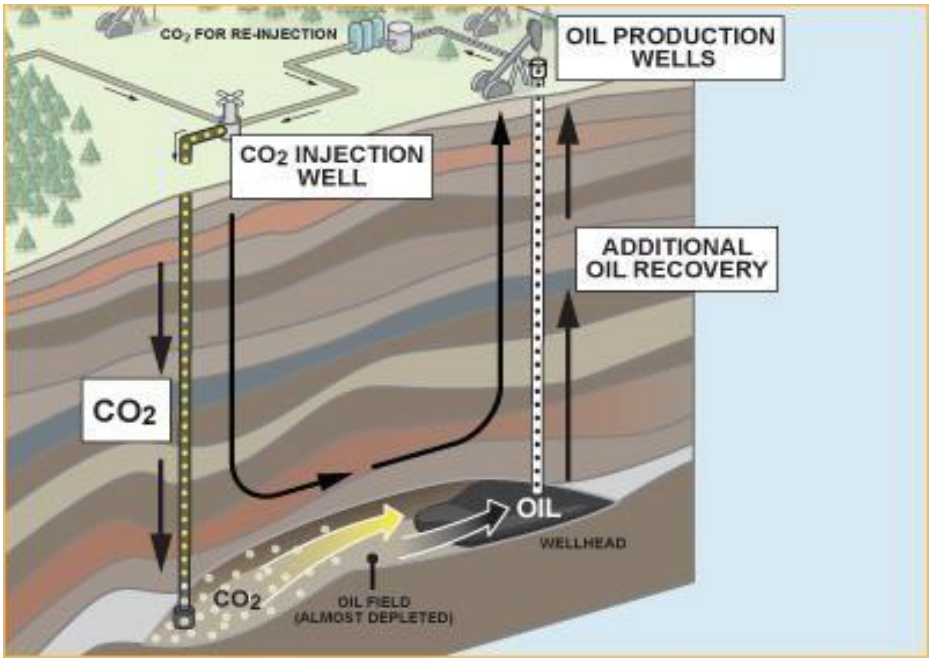

Figure 2-5. Onshore CO_2 based enhanced oil recovery [28]

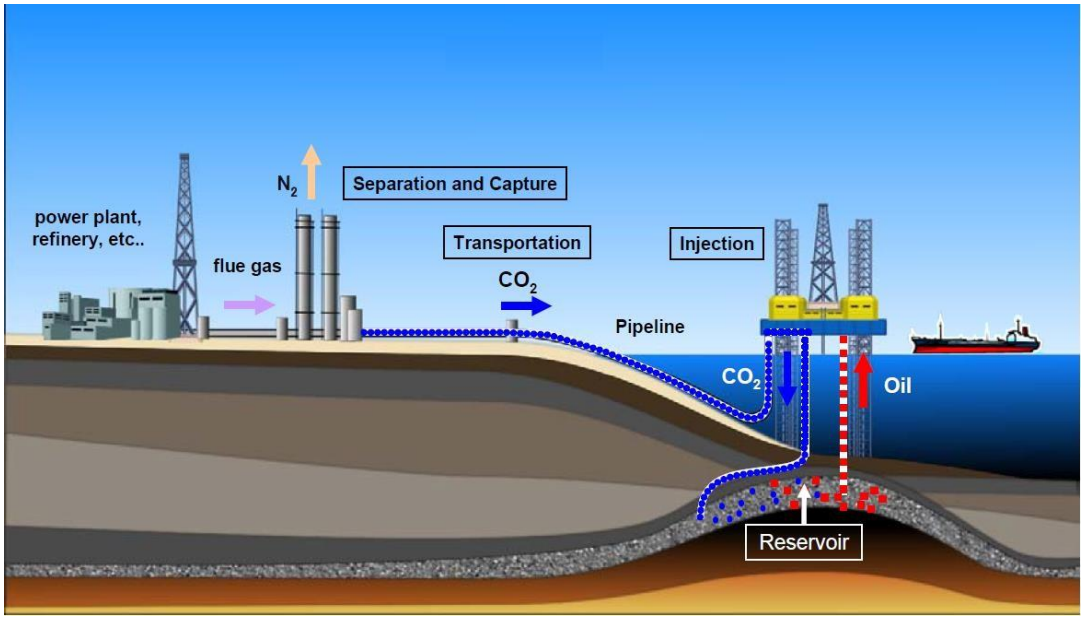

Figure 2-6. Offshore CO_2 based enhanced oil recovery [29]

From a theoretical point of view, miscible CO_2 flooding may displace all oil from a reservoir. However, in practice, it is complicated by heterogeneities of the formation, cracks that occurred naturally, and an adverse mobility ratio (M >1) during displacing process. In addition, CO_2 contact with oil in clusters or dendritic pores can be sophisticated by high water saturation. Drops of oil that have been coated by water cannot be displaced, leading to high residual oil saturation.

2.3.6 Limitations of CO_2 Injection

As already discussed, CO_2 is a good choice for EOR purposes. However, its miscibility is not appropriate for all reservoirs. If CO_2 is injected into the reservoir in which the oil is rich in aromatics, or, in other words, with a low API gravity, miscibility may not develop regardless of applied pressure. Instead, the two-phase liquid phases will be developed which are rich in CO_2 and have approximately the same viscosity. As a consequence, they will be displaced at almost the same rate. It leads to the recovery factor that may be the same as in the case of the miscible flow [5].

In the event of CO_2 injection, this can also lead to the precipitation of asphaltenes from oil, which is called as either a Vapor-Liquid-Liquid Equilibrium (VLLE) or a Vapor-Liquid-Solid Equilibrium (VLSE) system and wax deposition [27].

It is frequently encountered in practice the injection of CO_2 is performed after water flooding which had been lasting for a long period of time. In such cases, high water saturation is expected and must be taken into account during the analysis.

Table 2-1. The characteristics of the main EOR techniques [22]

EOR Technique	Working Principle	Outcome/ Results	When to use	Recovery rate
Gas Injection	Injecting gas or nitrogen (immiscible)	Push out crude or thins it, reduce rock-oil surface tension	Follow-up to water injection development (WAG- Water Alternating Gas Injection)	35% (variable)
Thermal Injection	Heat is injected to the reservoir to reduce the viscosity of the oil	Oil becomes lighter and flows more easily	Heavy crude fields	Up to 70%
Chemical Injection	Different type of chemicals (Polymers, Surfactants and others)	- Reduce interfacial tension - Increase flooded water viscosity	Follows waterflood to capture residual oil; Sandstone reservoir and less Limestone	Up to 15% incremental
CO2 Injection	Injecting Carbon Dioxide (CO2)	CO2 swells oil and reduce viscosity	Follows waterflood to capture residual oil (generally used in Limestone reservoir)	Up to 15% incremental

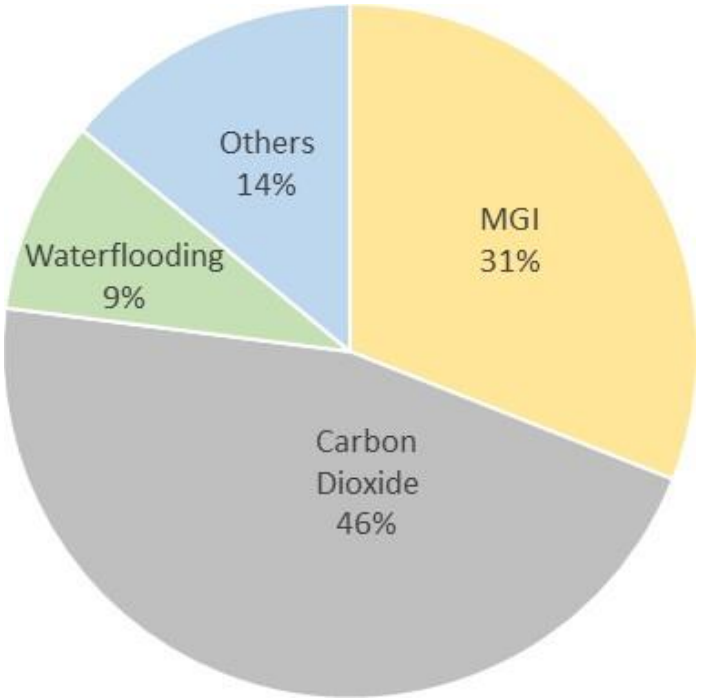

Figure 2-7. Examples of EOR opportunities offshore Malaysia [30]

2.4 Diffusion

2.4.1 Theoretical background

The process of gradual motion of concentration within a body, without net movement of matter as in the case of bulk flow, due to a concentration gradient is called diffusion. Bulk flow- the movement of a whole-body that occurs due to a pressure gradient [31].

Diffusion results in a gradual mixing of material. It is characterized by the net flux of molecules from a region of higher concentration to one of lower concentration.

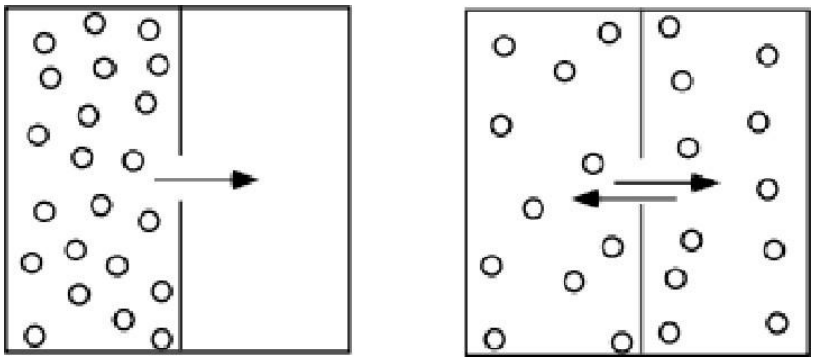

Figure 2-8. Mass transport, diffusion as a consequence of existing spacial differences in concentration

However, it is worthwhile to emphasize that diffusion also takes place in the case of the absence of a concentration gradient. Nevertheless, in the majority of cases, diffusion occurs in the presence of a concentration gradient. The property variation as a function of distance is referred to as a gradient. In case of linear variation of concentration of the material, the concentration gradient is constant. It can be determined as the slope of concentration change as a function of distance (dC/dx).

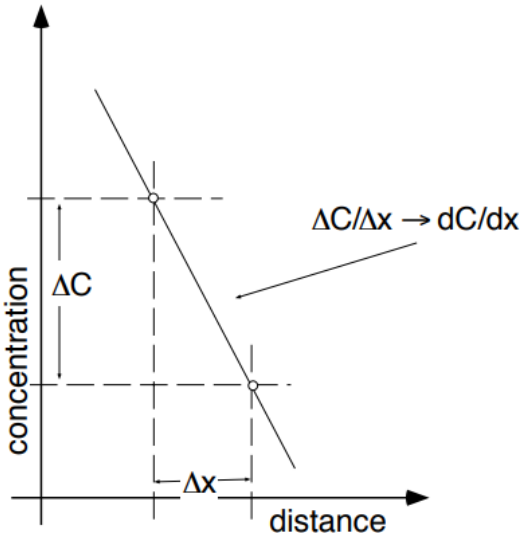

Figure 2-9. Concentration gradient (constant) in the x direction

The flux of each diffusion process (J), the dimension of which is the amount of substance per unit area per unit time (mol m^{-2} s^{-1}), can be described by the following relation:

$$J = -D \frac{dc}{dx} \tag{7}$$

The conductivity term, in the case of molecular or atomic diffusion, is defined as diffusion constant and introduced as a symbol "D" the dimension of which is area per unit time (m^2/s). Diffusion constant represents the mobility of the diffusing particles in accordance with the given environment which is large in gases, small in liquids, and extremely small in solids [32].

In the same way, the diffusion process between two miscible liquids forms a uniform solution. For instance, during the mixing of water with glycerol, the radial diffusion of two liquids into each other takes place over time. Observation of this process can be achieved by adding dyes to each liquid. However, the same procedure is not observed in the case of immiscible liquids such as petrol and water. For immiscible liquids, the diffusion process takes place only along the surface of interaction with a slow rate [33].

In many cases, diffusion is carried out in combination with other phenomena. If the rate of diffusion is the slowest in comparison with other phenomena, it confines the overall speed of the process. For instance, agitation can accelerate the rate of diffusion in gases and liquids. As an example, if the copper sulfate is stirred, the complete mixing can be achieved in a few minutes. The acceleration of mixing is associated not only with diffusion but with diffusion and stirring. The agitation or stirring is a macroscopic process but not a molecular one that shifts fluid portions to a much greater length. When the macroscopic movement occurs, diffusion mixes the newly contiguous fluid portions. In the case of the spread of pollutants, the agitation of wind or water creates an action similar to diffusion. This is referred to as dispersion [32].

2.4.2 Factors Affecting Diffusion.

The diffusion process is affected by the following factors [33]:

- Temperature
- Area of interaction
- The steepness of concentration gradient
- Particle size

The rate of diffusion can be altered by each individual factor or by their combination.

2.4.2.1 Temperature

The movement of all molecules in any system is accompanied by kinetic energy. The collision of molecules triggers changes in the direction, momentum, and velocity. For instance, in the case of placing dry ice block inside a box, CO_2 molecules in the center of the block will collide and hold in the solid mass. Nevertheless, the molecules at the edges of the block are affected by rapidly moving molecules in the air, which allows their diffusion into the air. As a

consequence, the concentration gradient is created at which CO_2 concentration decreases with distance.

An increase in temperature leads to an increase in the kinetic energy of all particles in the system. This results in a rise in the speed of movement of the molecules of the solute and solvent. This signifies that the vaporization of dry ice will occur faster at high temperature, due to the fact that molecules will move with more energy and are more likely to quickly break out of the solid [33].

2.4.2.2 Area of Interaction

Breaking dry ice blocks into several pieces will increase the area of interaction with the atmosphere. As a consequence, the number of molecules that collide and are held in the solid mass of CO_2 decreases, and the diffusion of gas into the air increases.

The observation of this property can be improved with odor or color gas. For instance, in the case of iodine sublimation, violet vapors appear and then mix with air. If sublimation is performed in a narrow container, the vapors slowly diffuse towards the top of the container and then quickly “disappear”.

Likewise, this is seen in the case of mixing two liquids. The area of interaction between two liquids can be increased by stirring which leads to an increase in the diffusion of these molecules to each other. Consequently, the reaction completes at a faster rate [33].

2.4.2.3 Steepness of Concentration Gradient

Insofar as diffusion depends, first of all, on the probability of the relocation of molecules from an area with a higher concentration, therefore, in the case of a very low concentration of solute in the medium or solvent, the diffusion of molecules from the central region is large. As an example, if the sublimation of

iodine in the crucible is achieved by placing it into another container this will lead to a decrease in the rate at which the purple gas "disappears" from the top of the crucible. The obvious deceleration is related to the fact that as time passes the container becomes saturated with iodine gas and some molecules will move rearward to the crucible. Despite the fact that the large bulk movements are random, there is a likelihood of a lack of net movement of gas from the container [33].

2.4.2.4 Particle Size

For a given temperature, the diffusion of small particles occurs more quickly in comparison with large ones. The reason for this is that large molecules have a larger surface area and are heavier, which reduces the rate of diffusion, while in small particles the diffusion process is accelerated. For instance, the diffusion of gaseous oxygen will take place faster than carbon dioxide, while their diffusion rates are higher compared to iodine gas [33].

2.4.3 Diffusion Coefficient

The importance of the diffusion coefficient is to provide information about the system. Due to the fact that different substances possess different diffusion coefficients their definition will give an idea about the matter. The diffusion coefficients at room temperature vary in the range 0.6×10^{-9}- 2×10^{-9} m^2/s [34]. The change in system properties will lead to an alteration of the diffusion coefficient. For instance, increasing the temperature of the system results in the enlargement of the diffusion coefficient. This is due to the fact that molecules have a larger thermal movement. There is also a correlation between the diffusion coefficient and the viscosity of the solution. The lower the viscosity, the higher the diffusion coefficient.

The dependence of the diffusion on the temperature can be described by applying the "Arrhenius" equation [35]:

$$D = D_0 \ e^{-\frac{E_a}{RT}} \quad (8)$$

Where,

- D is the diffusion constant
- Do is the maximal diffusion coefficient
- Ea is the activation energy for diffusion
- T is the absolute temperature
- R is the universal gas constant

The viscosity dependence of the diffusion coefficient can be characterized by the Stokes-Einstein equation [36]:

$$D = \frac{kT}{6\pi\eta r} \quad (9)$$

Where,

- k is Boltzmann's constant
- η is the dynamic viscosity
- r is the radius of the spherical particle

Coefficient of viscosity is defined by:

$$\eta = \eta_0 \ e^{-\frac{E_a}{RT}} \quad (10)$$

The temperature dependence of viscosity is demonstrated by this equation.

During heavy oil production, it is common to inject the solvent with the aim to reduce its viscosity by mixing with it. The rate of the mixing process is governed by the diffusion coefficient. Consequently, the diffusion coefficient is one of the most important parameters and proper diffusion data are required to determine:

- The amount and flow rate of solvent required to inject into a reservoir

- The portion of reserves that have been affected by the solvent undergo viscosity reduction
- The time required by the reserves to become less viscous and more mobile as desired
- The rate of live oil production from the reservoir

The determination of the diffusion coefficient relies on the experimental measurements since there is no universal theory that would allow their exact a priori determination. Unfortunately, the performance of experimental measurements is difficult with the variable quality of the results [37].

The assumption of constant diffusion coefficient is acceptable in many cases, particularly in the case of gas diffusion. Nevertheless, this is unacceptable in the case of dense and complex fluids. In order to apply constant diffusion coefficient theory for solvent/heavy oil system three conditions must be executed. If any of these conditions are not met, the diffusion coefficient is not expected to be constant and will be function of concentration. The conditions are the following [38]:

- Dimensions and shape:

The molecular similarity in dimensions and shapes are required. This means that the molecules of solvent and heavy oil should exhibit similarity in shapes and dimensions. For the solvent/ heavy oil system this assumption is not valid due to the presence of large hydrocarbon chains in heavy oil and taking into account that injected solvents are light gases with small hydrocarbon molecules.

- Molecular interactions:

Diffusing components should have negligible molecular interactions. This means that the forces of repulsion and attraction should not be involved in the diffusion process, despite the fact that repulsive forces play a key role in the diffusion process.

- Non-reacting environment:

The non-reacting environment is required in the system. This means there should be no transformations of components and/or conditions (pressure and temperature) in the system. However, the interaction of solvent with heavy oil can sometimes be accompanied by asphaltenes precipitation.

2.4.4 Multi-Component Diffusion

In the presence of more than one chemical substance with a significant number of mass fractions, for instance, concentrated solutions or gas mixtures, the assumption of a constant diffusion coefficient or independent of the composition is not suitable. Inter-molecular dependencies are no longer can be ignored by reason of the prevalent interactivity of molecules of different species. As a consequence, the diffusion equation should be altered and the diffusion coefficient becomes a tensor. The reason for that is the relation of the mass flux of one chemical species to the concentration gradients of all chemical species that are present. The appropriate equations were modeled by Maxwell-Stefan [39].

$$\nabla x_i = \sum_{j=1}^{N} \frac{x_i x_j}{D_{ij}} \tag{11}$$

Where,

- D_{ij}- multi-component diffusion coefficient

A reasonable choice of dependent variables, in Maxwell-Stefan diffusion equations, is the species mole (x_i) or mass fractions (ω_i) rather than concentrations.

$$\sum_i x_i = 1 \sum_i \omega_i = 1 \tag{12}$$

They are related to the concentrations and each other through the following equations:

$$x_i = \frac{c_i}{\sum_j c_I} \qquad \omega_i = \frac{M_i c_i}{\sum_j M_j c_j} \qquad x_i = \frac{\omega_i}{M_i \sum_j \frac{\omega_j}{M_j}} \tag{13}$$

Where,

- M_i- the relative molecular mass of species i

In the Maxwell-Stefan equation, the diffusive mass flux is expressed through gradients of mass or mole fractions by means of multi-component diffusion coefficients (D_{ij}). If the system consists of n number of components, n(n-1)/2 number of independent coefficients are required in order to parameterize the diffusion rate. These values are unknown for a system with four or more components. In this case, assumptions should be employed in order to simplify the Maxwell- Stefan equations to the equivalent Fick's law diffusivity [40].

2.4.5 Fick's Law

Factors affecting the diffusion rate of a gas through a liquid are demonstrated by Fick's law [41]:

- The pressure difference across the diffusion barrier
- The gas solubility
- The cross-sectional area of the fluid
- The distance that molecules need to diffuse
- The gas molecular weight

There are two types of diffusion processes:

- Steady-state
- Non-steady state

Both of them are quantitatively described by Fick's law. The first law applies to both steady-state and non-steady-state diffusion, while the second one is applicable only to non-steady-state diffusion.

4.1.1.1 Steady-State Diffusion (Fick's First Law)

Steady-state diffusion is a constant rate process that occurs when the number of molecules crossing the interface do not vary with time, in other words, dc/dx = constant and dc/dt = 0 all over the system. Fick's first law equation is the following [42]:

$$J = -D \frac{dc}{dx} \tag{7}$$

Where,

- J - the flux

Fick's first law postulates that the diffusion flux is proportional to the existing concentration gradient. If the values of the flux and the concentration variation over time know the diffusion coefficient (D) can be calculated. A negative sign in the equation denotes that the flow of particles is from a region with a higher concentration to a region of lower one [43].

4.1.1.2 Non-Steady State Diffusion (Fick's Second Law)

The process of non-steady-state diffusion is time dependent which is characterized by a variety of diffusion rates as a function of time. Therefore, dc/dx alters with time and dc/dt ≠ 0. Fick's second law is more applicable to the systems that are changing, such as physical science. Fick's Second Law [44]:

$$\frac{dc}{dt} = D \frac{d^2c}{dx^2} \tag{14}$$

If the concentration does not vary, then $d^2c/dx^2 = 0$

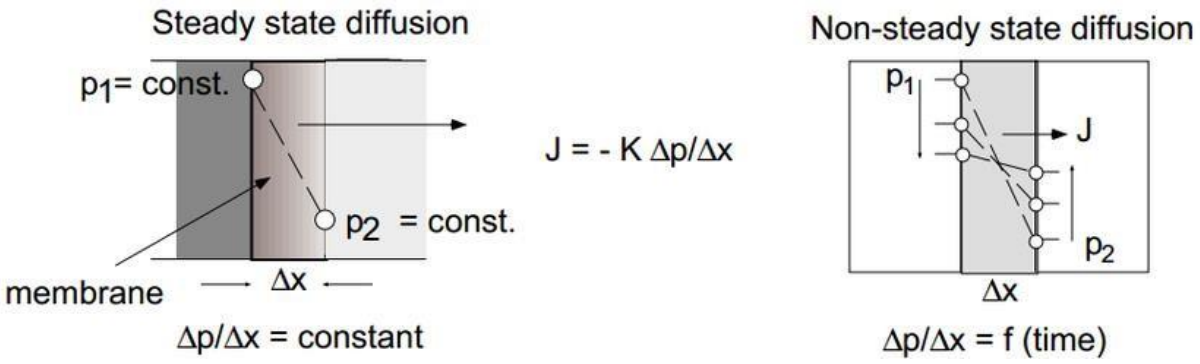

Figure 2-10. Steady-state and Non-steady state diffusion [45]

The difference between steady-state and non-steady state diffusion is depicted in the figure above. In the case of steady-state diffusion, the gas diffusion process takes place from an infinite volume (P_1=const.) through a membrane into an infinite volume (P_2= const.). This indicates that the pressure gradient across the membrane, as well as the diffusion flux, remain constant. In the case of non-steady state diffusion, the diffusion process takes place from a finite volume through the membrane into a finite volume. Consequently, the reservoir pressure changes over time, as does the pressure gradient across the membrane.

Fick's second law states that the rate of compositional alteration is proportional to the "rate of change" of the concentration gradient, not the concentration gradient itself [46].

2.5 Diffusion Coefficient Measurement Techniques

It should be noted that there is no universally applicable measurement technique of molecular diffusion coefficients, such as in case of viscosity or thermal conductivity measurements, for which there are standardized measurement techniques. Mass transfer characteristics measurement is generally more difficult. The complexity of it relies on difficulties of the concentration point values measurements as well as other issues that complicate the process of transportation. A lot of efforts have been dedicated to the experimental determination of diffusion coefficients in the process of solvent diffusion into the oil [47]. These experimental methods can be divided into:

- Direct methods
- Indirect methods

Direct Methods

In the case of direct methods, the diffusion coefficients are evaluated by measuring the concentration of the diffusing species as a function of penetration depth. These methods involve more reliability and a variety of physicochemical methods such as radioactive tracer technique, mass spectrometry, spectrophotometry, etc. The disadvantages of these methods are:

- High expenses
- Time consumptions
- System-intrusive

Indirect Methods

Indirect methods are based on measuring changes in one of the system parameters that affect the diffusion rate. The change of solution volume, pressure drop rate in a cell which is called pressure decay method in the cell, gas injection rate from top of the cell in by keeping the solution volume and pressure constant, magnetic field characteristics, computed tomography (CT) analysis are examples of indirect

methods. The advantage of this method is that there is no need to determine the composition change.

2.5.1 Pressure Decay Method

In comparison with other indirect methods, due to its simplicity pressure decay method has attracted more attention. During this method, gas (as a solvent) and oil are injected into a cell. In the beginning, the fluids in the cell are at a non-equilibrium state. As time passes, gas dissolves into the oil which results in the pressure reduction in the cell. The amount of transferred gas into the oil, as well as the diffusion coefficient, can be determined by recording the pressure and the level of the liquid in the cell. The failure of the pressure decay method occurs in case of complex hydrocarbon mixtures with multiphase behaviors [48].

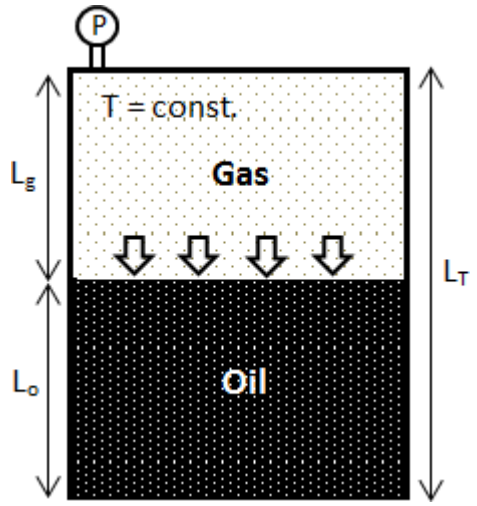

Figure 2-11. Pressure Decay Test Cell

This method was first applied by Riazi for the dissolution of methane in n-pentane [49]. The non-equilibrium gas into contact with n-pentane was taken in a container with a constant temperature. The assumption of thermodynamic equilibrium at the gas-liquid interface was made. Nevertheless, the pressure, as well as the interface position, may vary with time. The rate of pressure and interface position variation with time depends on the diffusion rate and, as a consequence, on the diffusion coefficients.

Different mathematical solutions have been proposed and developed by other researchers by differently modeling the interface boundary condition. However, complex mathematical solutions are often required for modeling the physics of the interface during the pressure decline, and the assumption of constant equilibrium concentration at the interface triggers significant errors in diffusion coefficient calculations. These shortcomings have been overcome by different researchers using different models.

2.5.2 Refractive Index Method

The ratio of the velocity of the wave in a reference phase to the one in the phase of interest is known as the refractive index[50]. Generally, the refractive index for diffusion measurement is taken as the ratio of the velocity of light in a vacuum to the velocity of light in the relevant phase:

$$n = \frac{c}{v} \tag{15}$$

Where,

- c - velocity of light in vacuum
- v - velocity of light in the relevant phase
- n - refractive index

In case of choosing the velocity of light in vacuum as the reference, the value of the refractive index is always greater than 1. For instance, the meaning of the refractive index of water equal to 1,33 means that the light travels 1,33 times faster in a vacuum than in water. When light moves from a medium, such as water, glass, or air into another one it can change its direction of propagation as well as refractive index.

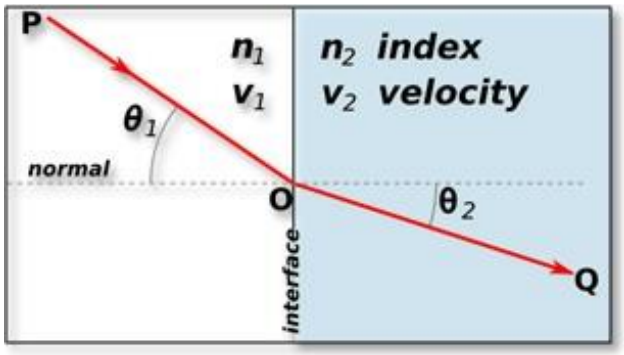

Figure 2-12. Refraction of Light at the Interface between Two Media

Snell's law is a formula which describes the relationship between the angles of refraction and refraction index, when light or other waves pass through an interface of two different media, such as two fluids with different solvent concentrations.

$$\frac{\sin\theta_1}{\sin\theta_2} = \frac{v_1}{v_2} = \frac{n_2}{n_1} \tag{16}$$

Where,

- θ - the angle of refraction

It should be noted that different refractive indices will be obtained for a solution with different concentrations of the sample substance. As a consequence, the concentration of a solution phase can be determined from the angle of refraction. Generally, in experimental measurements of refractive indices, the diffusion cell is emitted by laser light, and the refractive angle of the laser beam is determined in accordance with the concentration of the solution at each elevation. As a result, the concentration in the diffusion cell at the specific elevation can be determined by the point at which the laser beam is captured by a CCD camera.

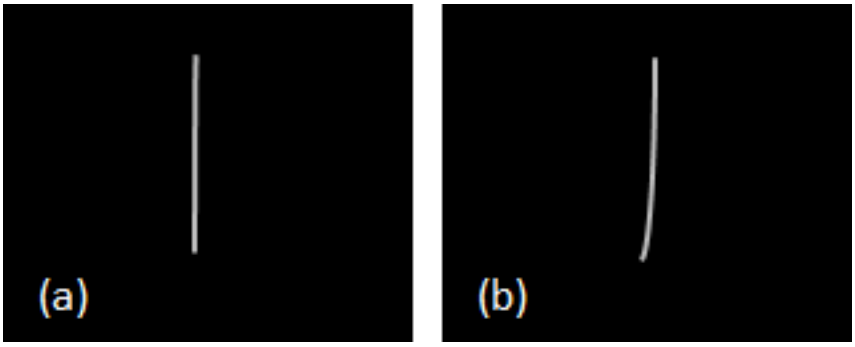

Figure 2-13. Sample of Light Refraction Results a) Initial Time, b) After Diffusion Occurred

The above process is only appropriate for translucent fluids. Since heavy oil is transparent, even if diluted, this method cannot be used. Nevertheless, this method is applicable only in case of transparent fluids. In case of heavy oil, even if it is diluted, it is opaque; this method cannot be applied.

2.5.3 NMR Method

Nuclear Magnetic Resonance (NMR) was developed for physical-chemical-medical use. This method is based on the calculation of the density of hydrogen protons.

NMR is a phenomenon, which takes place when the cores of certain atoms are submerged in a static magnetic field and subjected to a second oscillating magnetic field [51]. Some of the nuclei may experience this phenomenon while others do not, which depends on the atomic composition. Depending on the magnetic resonance nature, NMR measurement can be performed on a core that has an odd number of neutrons or protons, or both, such as the core of hydrogen (H), carbon (C) and sodium (Na). For the majority of the cores found in earth layers, external magnetic fields induce a too small the nuclear magnetic signal to be detected using an NMR device, such as the borehole NMR logging tool. Nevertheless, hydrogen produces a strong signal, which is the main component of

water and hydrocarbon molecules. As a consequence, the signal strength can be used as a scale of the present hydrogen.

2.5.3.1 Application of Low Field NMR in Diffusion Measurements

The difference in the relaxation spectra of heavy oil or bitumen compared to the solvent is the basis of using NMR.

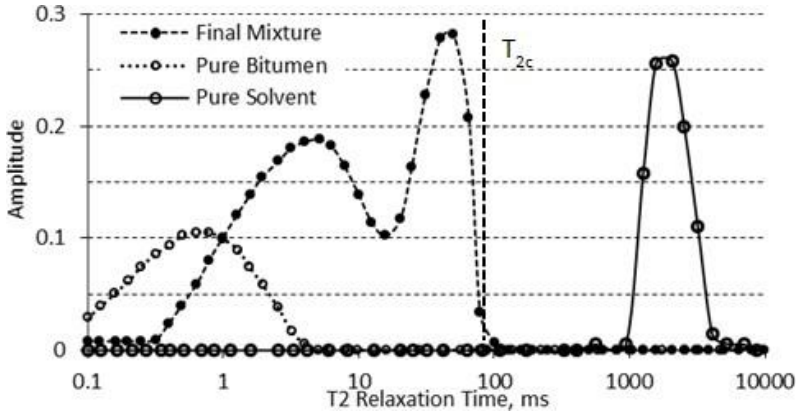

Figure 2-14. Typical NMR Spectrum for Pure Bitumen, Pure Solvent, and a Mixture

Through mild heating and stirring, the spectra of a pure solvent, pure viscous oil, and a mixture were prepared, as shown in Figure 2-14. It can be observed that the amplitude indices of the signals from solvent (AIS) are higher in comparison with the amplitude indices of the bitumen signals (AIb). The reason for this is that the bitumen molecules are large, which leads to a smaller amount of hydrogen per unit volume compared to a solvent that has a smaller molecular size. On the other hand, the relaxation time of bitumen is much faster than a solvent, due to the high viscosity of the bitumen. It can be noticed that the spectra of the individual components are different from the spectrum of the mixture. This distinction underlies the methodology used to study solvent diffusion in heavy oil using NMR [52].

According to Figure 2-14, as diffusion of a solvent into the bitumen takes place the bitumen spectrum moves to longer relaxation time by decreasing its viscosity,

while the spectrum of solvent moves to faster relaxation time by increasing its viscosity. This results in one continuous multi-peak spectrum.

Prior to initiating the experiment, the mixtures are prepared with the known percentages of solvent and bitumen after which the correlation between bitumen concentration in the mixture and the NMR parameters is determined (calibration of NMR parameters with bitumen content). Using these correlations leads to the calculation of solvent concentrations diffusing into the bitumen during the test.

$$m_{sb} = {}^{A_{sb}}/_{AI_s} \tag{17}$$

Where,

- m_{sb} - Mass of diffused solvent into the bulk
- A_{sb} - Bulk solvent signal amplitude
- AI_s - Pure solvent amplitude index

The mass of diffused solvent can be calculated through the following relation:

$$m_{sd} = m_s - m_{sb} \tag{18}$$

Where,

- m_s - Mass of initial pure solvent
- m_{sd} - Mass of diffused solvent

Calculation of the total amplitude of the diffused solvent can be performed using the following relation:

$$A_{sd} = A_s - A_{sb} \tag{19}$$

Where,

- A_s - Total pure solvent amplitude
- A_{sb} - Total bulk solvent amplitude

The combined diffused solvent and bitumen/oil amplitude index is calculated using the definition of the amplitude index:

$$\frac{A_{db}}{(m_b + m_{sd})} = AI_{db} \tag{20}$$

Where,

- A_{db} - Signal amplitude of diluted bitumen
- m_b - Mass of pure bitumen
- m_{sd} - Mass of diffused solvent
- AI_{db} - Amplitude index of diluted bitumen

The solvent concentration can then be computed by creating a correlation at different times between NMR properties and bitumen contents.

The solvent concentration determined by the NMR spectrum changes in the mixture area is the overall concentration, C, and depends on the time and diffusion coefficient. In the following equations the correlation between concentration *C*, time *t* and *D* is defined:

$$C = f(x, t, D) \qquad \int_0^l C dx = \int_0^l f(x, t, D) = g(t, D) \tag{21}$$

At given t:

$$\bar{C} = \frac{\int_0^l C dx}{\int_0^l dx} = \frac{\int_0^l f(x, t, D)}{l} = g(t, D) \tag{22}$$

With the aforementioned equation, C with D and t models can be constructed and the coefficient of diffusion can be estimated. During each small time interval, the D value is assumed to be constant in the NMR test. As a consequence, for the determination of the diffusion coefficient, the following equation could be used:

$$C = \frac{1}{2} C_0 \operatorname{erfc}\left(\frac{x}{2\sqrt{Dt}}\right) \qquad (23)$$

Where,

- C_o - Starting concentration
- x - The equilibrium distance for the early times (for example first two days) of measurements
- D - The diffusion coefficient that gives the best fit

The results of the diffusion coefficient, calculated using the NMR experiment, are shown in Figure 2-15.

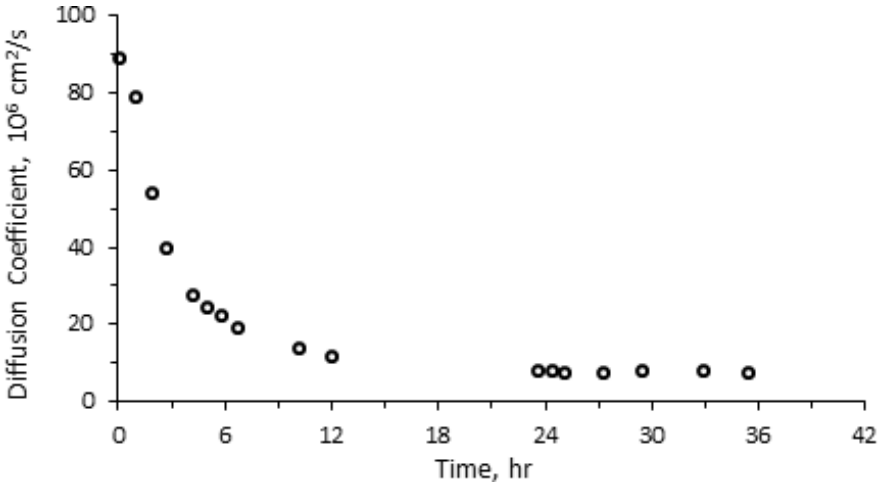

Figure 2-15. Diffusion Coefficient as a Function of Time (NMR Experimental Result)

2.5.4 Computer-Assisted Tomography.

In reservoir rock characterization and fluid flow visualization, computer-assisted tomography (CAT) scanning by X-ray has extensively been used in research laboratories around the world.

X-rays lose their energy when transiting a medium, and this decrease is affected by the density of the substance and its path length.CAT is based on the emission of x-rays from a source around the object, while a detector on the other side of the source recording a one-dimensional projection of attenuated x-rays [53]. These screenings are taken as the sample moves longitudinally through the scanner and used for the reconstruction of a two-dimensional image of the specimen.

Attenuated x-rays intensity values are gathered from tiny volumetric elements, known as pixels. Typically, these elements are 0.40 per 0.40 mm and 3 cm in depth for the second-generation CAT scanner (along the direction of the ray beam).

After a full radial and longitudinal scan, these elements are all given intensity values, which are then processed by a computer. The main part of the CAT is constituted by this processing. By the following relation, the inlet intensity and outlet intensity are connected:

$$\frac{I}{I_0} = \exp(-\mu L) \tag{24}$$

Where,

- I - The intensity remaining after the X-ray passes through a thickness (kV)
- I_0 - The incident X-ray intensity (kV)
- μ - Linear attenuation coefficient
- L - Path length

This is only true for a narrow monoenergetic beam of x-ray photons that travels a uniform medium. In case of a heterogeneous medium, the above-mentioned equation can be applied while substituted by the line integral of the linear attenuation coefficients.

The modified form is:

$$\ln\left(\frac{I}{I_0}\right) = \int_s^d \mu(x, y)dL \tag{25}$$

The following equation relates the linear attenuation coefficients to the number stored in the computer (known as the CT numbers or CTn):

$$CTn = \frac{1000 \times (\mu_i - \mu_w)}{\mu_w} \tag{26}$$

Where,

- CTn - CT number
- μ_i - x-ray linear attenuation coefficient of the object scanned
- μ_w - x-ray linear attenuation coefficient of water

Linear attenuation coefficient (μ) is a function of the effective atomic number and the bulk density of the sample, given by:

$$\mu = \rho\left(a + \frac{bZ^{3.8}}{E^{3.2}}\right) \tag{27}$$

Where,

- ρ - Bulk oil density
- a - Energy-independent coefficient known as Klein-Nishina coefficient

- b - Constant
- Z - Effective atomic number of the sample
- E - Mean photon energy (kV)

A transmitted intensity vs. elevation curve (Figure 2-17) can be built when subjecting a medium to x-rays, collecting exiting x-rays from the medium (Figure 2-16) and by averaging intensity for every cross-section. Depending on the relationship between x-ray intensity and density, the resulting curve could be converted to a density curve.

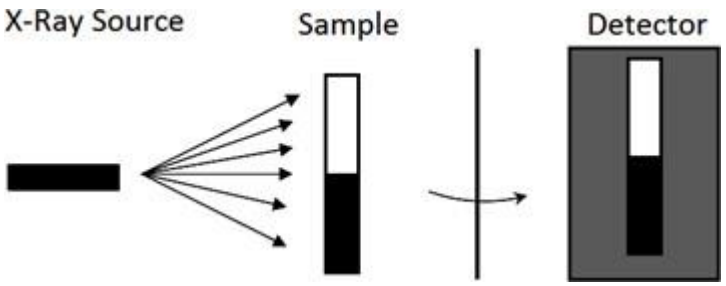

Figure 2-16. Schematic View of CAT Scanning Using X-Ray

Calibration tests series for liquid and solid samples of known densities are carried out to correlate the CT numbers, which are generated by the scanner, to densities. For liquid samples and liquid/solid samples, calibration curves are demonstrated respectively in Figure 2-17. The densities of the scanned samples can be determined with the aid of these calibration curves. This method has the capability to work with opaque solutions such as bitumen and pentane in contrast to the refractive index method.

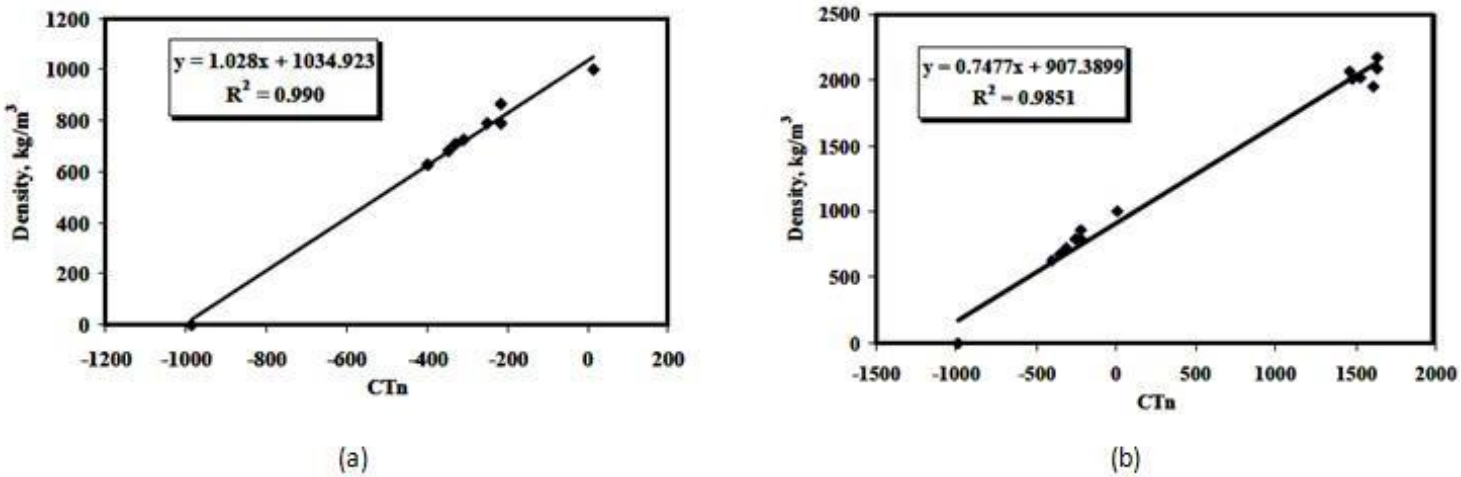

Figure 2-17. Calibration Curves for the CAT Scanning, (a) Liquid Calibration Curve, (b) Liquid-Solid Calibration Curve [53]

2.6 Experimental characterization of diffusion coefficient.

2.6.1 Radial Constant Volume Diffusion (RCVD) Method.

2.6.1.1 Introduction

This laboratory work [54] aimed to fill the gaps experimentally using the Radial Constant Volume Diffusion (RCVD) approach to examine diffusion coefficients in hydrocarbon-saturated porous media at different pressures.

At first, the core becomes saturated with oil, while at the same pressure the annulus was filled with CO_2. The system pressure decreases as the gas diffuses into the oil phase until the chemical equilibrium is reached. The history match of the pressure decline curve was performed in order to determine the diffusion coefficient. The initial pressure of the system is 597 psi, and the determination of the diffusion coefficient was carried out in numerical models respectively. The estimation of molecular diffusion coefficients was executed at different periods of the experiment to display pressure dependence. When including molecular diffusion in reservoir simulations, models with various grid numbers are used to demonstrate the scale dependency.

As depicted in Figure 2-18, the diffusion coefficient measurements can be divided into three methods, based on pressure changes and gas mass transfer. Figure 2-18a displays the set-up configuration above the fluid-saturated core sample with a constant volume. Solely the top cross-section of the core can be reached by free gas; the other core sides are properly separated to maintain the non-flow boundary state. At the starting point, gas and oil are subjected to the same pressure. As soon as the diffusion process begins to occur, the pressure in the system decreases. The pressure drop curve is the basic data gathered to estimate the diffusion coefficient [55], [56], [57]. In Figure 2-18b, the configuration is similar to the one in Figure 2-18a, except that constant pressure boundary condition is applied in the gas phase. As the diffusion takes place, the height of the free gas reduces and the

amount of the injected gas can be estimated, which is the main data used to calculate the diffusion coefficient [58]. The configurations of Constant Volume Depletion (CVD) and Constant Pressure Depletion (CPD) are distinguished by a concomitant cycle involving gravity-drainage convection that contributes to a rapid decrease in pressures compared to a single present molecular diffusion. As pointed out by Renner, the diffusion coefficient is smaller when the core cell is placed horizontally and not vertically when using the CPD system [58]. Conversely, the design of the configuration in Figure 2-18c instead reduces the effect of gravity drainage convection phenomena. As Figure 2-18c illustrates the top and bottom sections of the core are sealed, whilst the lateral surface is subjected to free gas. Similarly, the data of the recorded system pressure decrease will also be used to measure the coefficient of diffusion.

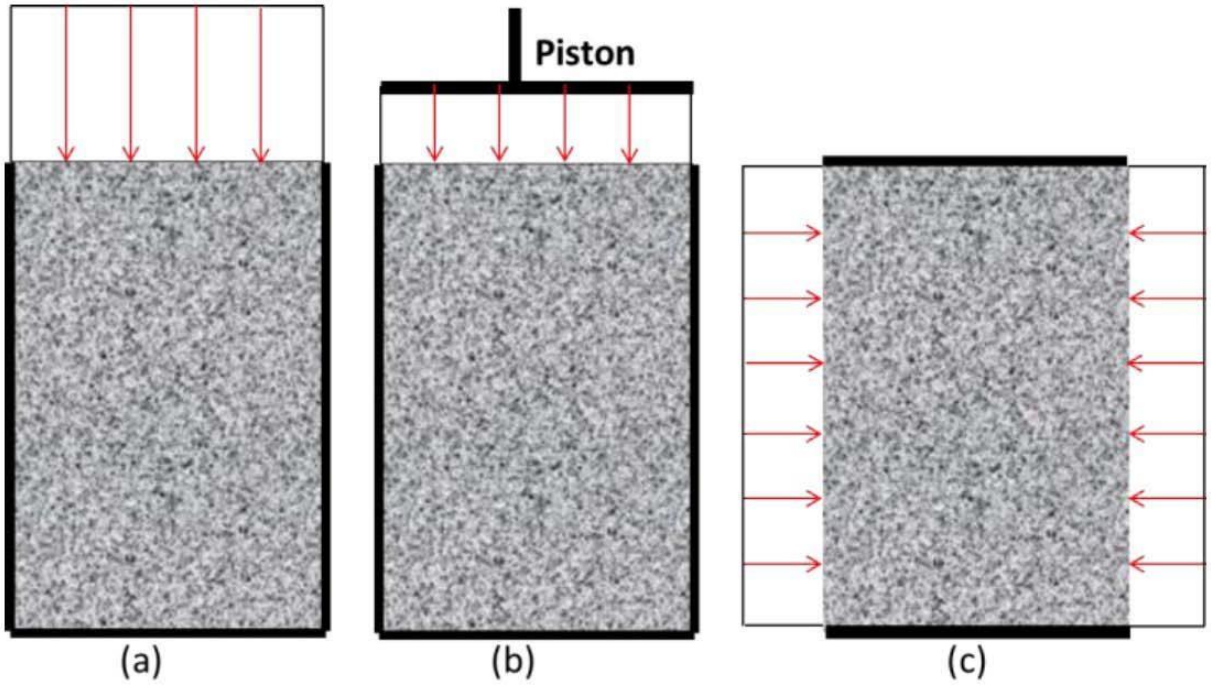

Figure 2-18. Three main experiment set-ups of measuring gas diffusion coefficient in liquid-saturated porous media: (a) CVD [57], (b) CPD [58]; and (c) Radial Constant Volume Diffusion (RCVD) [56]. The thick black solid line represents the no-flow boundary condition that is exerted

The objectives of this study are:

- Simulate the RCVD system
- Measure the diffusion coefficient using different parts of the pressure

2.6.1.2 Experiment procedures

The core sample used in this study [54] has the following properties:

- Diameter = 1.5 inches
- Length = 2.3 inches
- Porosity = 19.7%
- Klinkenberg-corrected permeability =254 mD

The top and bottom cross-sections of the core sample are covered by epoxy such that only in the radial direction the mass transfer between gas and oil takes place.

Before free gas is pumped into the container, the surface coating is used to prevent diffusion of gas into the porous material from the distributor cap. The core cell design is depicted in Figure 2-19. For 3 days the epoxied core sample was dried under the required temperature in the oven, i.e. 104 °F in the present study. The core sample is positioned in the core cell as defined in steps 1-3 in Figure 2-19. There are three components in the core cell: a, b, c. In the leftmost image, the interface between the core and cap of the distributor (a) is presented: the distributor cap for the distribution of fluids is engraved with connected rings. In the right-hand picture, two effluent ports can be observed at the center and the annular space under the cell holder (b).

Figure 2-19 also demonstrates the experimental measurement set-up of the hexadecane saturated core sample for the gas diffusion coefficient. The connection of the core cell to the system is performed by means of plumbing blocks. The temperature of the oven is set to 104 °F. With the valve V_2 open to 14 psi, the entire system is vacuumed using the vacuuming pump. Once the

vacuuming pressure is reached on the P_2 transducer, assuring that pores in the core sample are vacuumed, the vacuuming process is initiated, which lasts for half an hour. When the vacuum pump ceases, the back pressure regulator (BPR) is loaded to the required level with nitrogen to reach the desired pressure. By dint of the Vindum pump, N-hexadecane is injected into a vacuum system. Constant flow rate mode is first implemented and the flow rate is slowly reduced with reaching the target pressure [59]. Afterward, constant pressure mode is applied with the pressure of 597 psi: the flow rate would oscillate before reaching zero, which indicates that no longer oil is able to be pumped. The next step is to close the valve V_2 and monitor the pressure for 3 hours to ensure no pressure changes. In this way, the lack of leakage in the system is confirmed. The pressure drop after gas injection is therefore triggered by the effect of diffusion. which is 104 °F in the current study.

The required temperature of the CO_2 ISCO pump, which is 104 in the current study, is reached by using a water-circulating temperature control system. The pressure of the CO_2 pump is set to 602 psi, which is 5 psi more than the required pressure. This step is taken to ensure there is no fluid flow back to the CO_2 pump when V_2 is open. Beyond opening V_2, the cell will be supplied with CO_2 at the selected constant flow rate mode, which is 10 mL/min. The annulus oil is leaked through the back pressure regulator (BPR). Once the annulus has been loaded with the free gas phase, V2 is shut down and the CO_2 pump is seized. As the amount of oil in the burette is no longer raised, the oil in the annulus has been drained entirely and closing of V2 is supposed to be done. The record of pressure change has been performed by means of three Heise pressure transducers which are located at the core cell inlet and outlet and the BPR dome. The resulting pressure reduction curve, which is recorded by the P2 transducer, is then interpreted as the main source for measuring the diffusion coefficient.

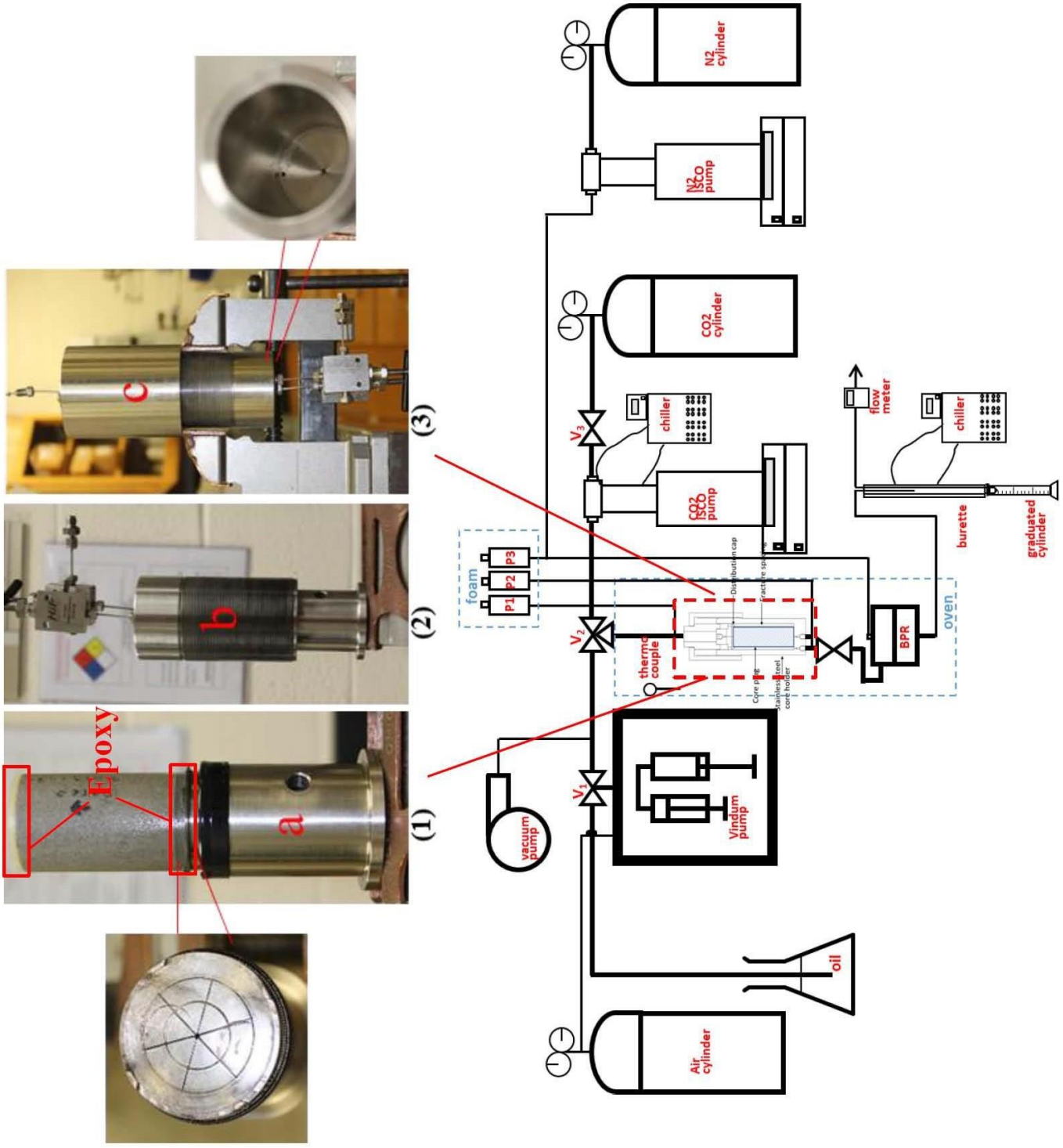

Figure 2-19. Schematic of the experimental set-up. The enlarged picture shows procedures of placing the core in the core cell: (1) place the core above the distributor "a", (2) carefully install distributor "a" into cell holder "b", and (3) invert the cell holder body, and close the cell with end cap "c"

2.6.1.3 Model set-up

Figure 2-20 depicts the model set-up in GEM [60]. The pore space is 100% saturated with oil (blue). The gas phase is around the core (red). In order to attain thermodynamic equilibrium due to the composition gradient, the gas diffuses in the oil phase, resulting in the pressure drop in the system. This pressure decline curve is the main source to acquire the diffusion coefficient of CO_2 by history matching. As demonstrated in Figure 2-20, the model has different grid numbers. The total grid numbers are 72, 162, 288, 450 for Figure 2-20a, b, c, and d, respectively. The grid numbers in the radial and longitudinal directions are represented in Table 2-2. This aim of using different grid numbers is to investigate the grid sensitivity to measure the diffusion coefficient. The initial conditions are:

- The system is under the same pressure
- The annulus is 100% filled with free CO_2
- The core sample is 100% filled with n-hexadecane

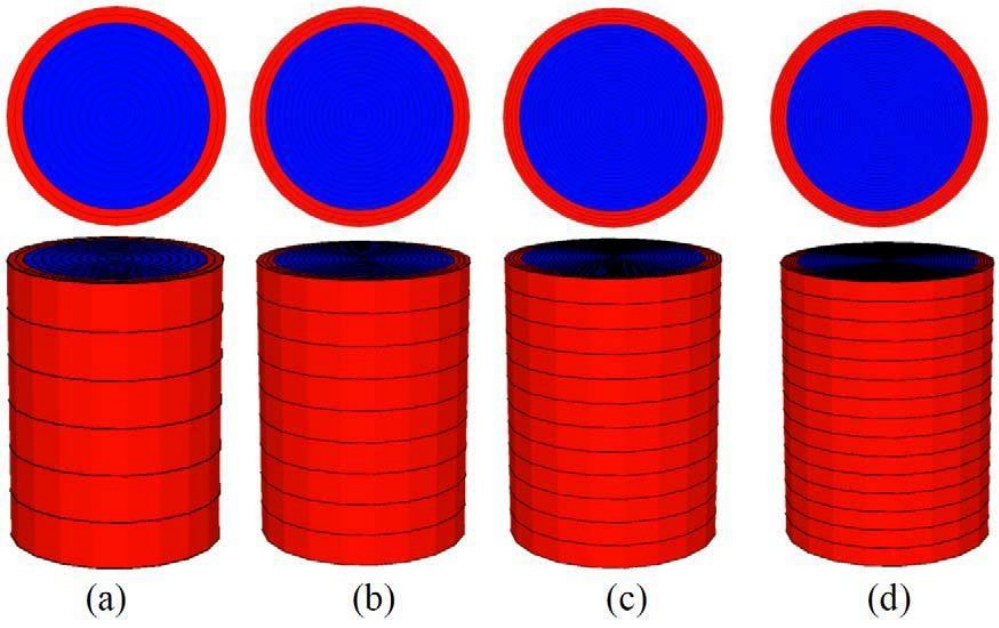

Figure 2-20. Six grid settings with 72, 162, 288, and 450 grids. The upper layer shows the surfaces and the lower layer shows the 3D settings; the red color represents the annulus, and the blue color represents the core: (a) 72 grids, 12×6; (b) 162 grids, 18×9; (c) 288 grids, 24×12; and (d) 450 grids, 30×15

Table 2-2. Grid system in four grid settings with 72, 162, 288 and 450 grids

	72 grids	162 grids	288 grids	450 grids
Radial/core	**10**	**15**	**20**	**25**
Radial/annulus	**2**	**3**	**4**	**5**
Longitudinal	**6**	**9**	**12**	**15**

2.6.1.4 Effective molecular diffusion coefficient

In the case of the injection of gas into the fractured reservoirs, cracks are first filled, where the diffusion of the gas phase into the oil phase plays an important role. The filling of cracks with the gas phase leads to a large composition gradient between the crack and the matrix. Therefore, molecular diffusion has great potential. Through the diffusion of the oil phase gas reaches the matrix when the matrix is primarily filled with oil, with or without the connate water saturation. Accordingly, the diffusion coefficient indicated in this analysis refers to diffusion in an oil phase, since the gas phase becomes saturated in the crack, and at the beginning of the experiment, the oil in the matrix is undersaturated. Furthermore, the effective value of the diffusion coefficient is obtained in this work, already considering the porous media. The effective value is lower in comparison with the bulk phase value since only a portion of the cross-section of the porous media is approachable for fluid flow, and the fluids travel paths are tortuous instead of straight.

Molecular diffusion flux in porous media between phase i and j can be expressed as:

$$J_i = T_d \, \emptyset \, S_c \, D_{eff} \, \Delta C_i \qquad (28)$$

Where,

- T_d – the diffusion flux
- $\emptyset$ – porosity
- S_c – saturation
- D_{eff} – the effective diffusion coefficient
- ΔC_i – the concentration gradient

At the interface between fractures and matrix blocks, there is a thin layer that serves as the contact zone which connects the oil and gas phases. Through this thin layer, the diffusion of CO_2 into the undersaturated oil takes place.

The direction of moving front is the key difference between the RCVD and CVD systems.

In case of the RCVD system, the moving front is heading to the top left of the half cross-section, as the denser oil is deposited at the bottom right corner, which is distinct from the one seen in the CVD system, in which gravity convection aggravates the diffusion. As a consequence, convection due to gravity is lower in the RCVD system compared to the CVD system in which the moving front is directed downward. On the basis of this, the major contributor to the decrease in pressure in the RCVD system should be molecular diffusion.

In the RCVD system, the diffusion coefficient calculation is not susceptible to capillary pressure curves, but a set of capillary pressure curves is still required. It was also noted that the measured diffusion coefficients are independent of the input of the capillary pressure curves of the CVD system when the substance that has been tested is dead oil [57]. In the CVD system, the moving front is directed downward, and together with gravity drainage, capillary pressure causes the convection that accelerates pressure decrease. Convection and diffusion could, therefore, be both necessary to facilitate a decrease in pressure.

The diffusion coefficient is a function of concentration and pressure, which continually changes during the diffusion process. The length of 174 minutes has

been split into three segments for the achievement of diffusion coefficients at various stages and to deliver improved curve fitting results, and each segment was independently fitted. Solely from the simulation results, the variance in the diffusion coefficient in a small grid-size model, with less dense distributed pressure curves, is more significant.

The diffusion coefficient as a function of the grid number depicted in Figure 2-21, from which the dependence of the diffusion coefficient on time and the grid number is revealed. The diffusion coefficient indicates a decreasing tendency and a plateau with increased grid numbers: the values vary slightly for 20 minutes and 30 minutes, segment 2 and 3 values no longer decline from the grids of 288 to 450

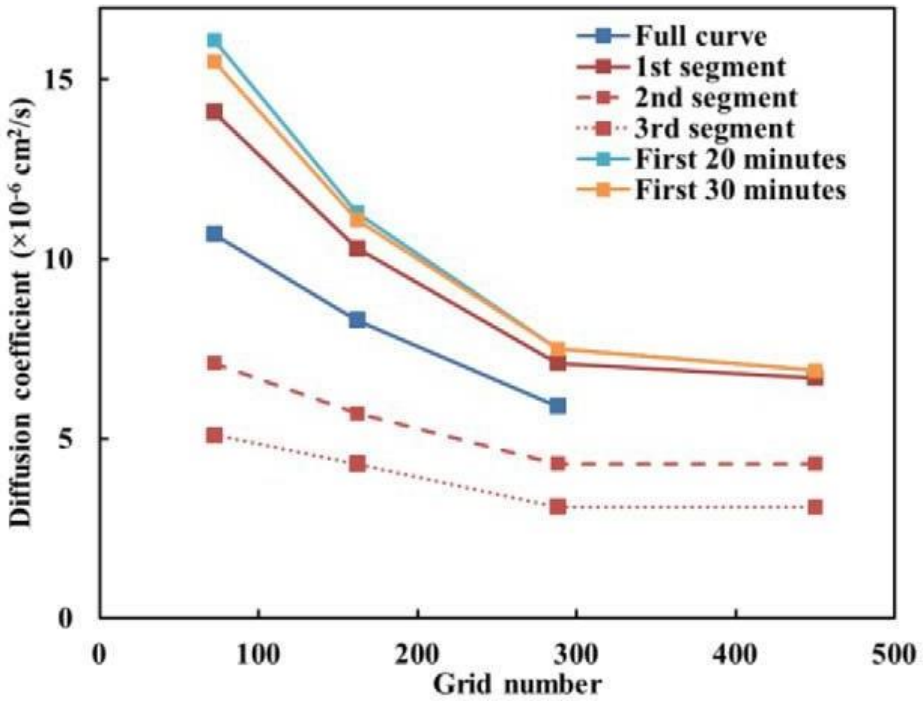

Figure 2-21. Plot of oil phase diffusion coefficients with different grid numbers

The variation of effective diffusion coefficients that are acquired by using different parts of the pressure curve specifies that as time elapses, the value of effective CO_2 diffusion coefficient reduces. The diffusion coefficient at the beginning of the experiment (6.7×10^{-6} cm^2/s) is twice as high as at the end of the

experiment (3.1×10^{-6} cm^2/s), based on the 450 grid model. While pressure reduces as the experiment goes, the observation also reveals that the effective diffusion coefficient becomes greater under higher pressure.

2.6.2 Computer-Assisted Tomography (CAT) and Pressure decay Methods.

2.6.2.1 Introduction

During this study, the attempts have been dedicated to determining the molecular diffusion coefficient for the CO_2-light oil system under various laboratory pressure conditions [61]. Both the techniques of pressure decay and computed tomography (CT) analysis are used for the experimental tests. The tests took place on a specially built vertical high-pressure cell. The temperature was 293.15 K, while various pressures were applied, which ranged from 2.76 MPa to 28.96 MPa. During the diffusion process, the swelling effect was also taken into account by monitoring the change in height of the oil column inside the cell.

The diffusion coefficients were acquired throughout the Etminan [62] interface resistance model using the CT method and pressure decay technique. The values of the coefficients differ significantly in both processes. It is worth emphasizing that the diffusion coefficients acquired from the pressure decay method are more compatible with published data. Thus, even for the CO_2-light oil mixture, the pressure drop method seems more reliable, while further improvements are required for the CT technique. Moreover, since Etminan [62] model is only suitable for VLE conditions, a modified model for LLE scenarios will be required.

Without laboratory experiments, it is very difficult to measure the molecular diffusion coefficient in a multicomponent system. Therefore, several methods for measuring the gas-liquid diffusion coefficient have been developed.

The purpose of this study is to determine the diffusion coefficient of CO_2 using the pressure decay method under various experimental conditions of pressure and composition in a porous medium saturated with light crude oil [61]. In addition to the technique mentioned above, in order to measure the concentration distribution over the oil phase, and to gain a comprehension of the whole process, the pressure cell was equipped into a CT scanner.

Table 2-3. Literature reported conditions

Researchers	System	P (MPa)	T (K)	Diffusion Coefficient	Swelling Effect	Compressibility factor	Boundary condition at interface
Riazi, 1996	C1-n-C5	7	311	Concentration dependent	Yes	PR-EOS	Equation (29)
Tharanivasan, 2006	CO_2-bitumen	4.2	297	Constant	No	Lee-Kesler correlation	Equation (30)
Haugen and Firoozabadi, 2009	C1-n-C5 C1-n-C12	7	311	Constant	Yes	PR-EOS	Equation (29)
Guo et al., 2009	CO_2-light crude oil system	20	333	Concentration dependent	Yes	PR-EOS	Equation (29)
Etminan et al., 2013	CO_2-bitumen	4	348	Constant	No	Constant	Equation (31)

$$C(z,t)|_{z=0} = C_{sat}[P(t)] \quad t > 0 \tag{29}$$

$$D\frac{\partial C}{\partial z}|_{z=0} = k\,[C_{sat}(P_{eq}) - C(z,t)|_{z=0}] \tag{30}$$

$$-D\frac{\partial C_g}{\partial z} = k\,[C_{g-int}(t) - C_g(z=0,t)] \tag{31}$$

The ability to control fluid movement in rocky bodies is one of the most important functions of CT. By the recorded CT numbers, CT recognizes density contrasts in the scanned specimen. The relationship between densities and CT numbers is direct. The following equations are used to acquire CT number-based concentration during liquid solvent diffusion into oil:

$$C_{sol} = \frac{\rho_{mix} - \rho_{oil}}{\rho_{sol} - \rho_{oil}} \tag{32}$$

$$C_{sol} = \frac{CT_{mix} - CT_{oil}}{CT_{sol} - CT_{oil}} \tag{33}$$

2.6.2.2 Pressure-decay model

Only after the following assumptions in Etminan work [61], for the model with interface resistance during the pressure decay experiment under isothermal conditions, the application of Fick's second law is reasonable:

- There is no chemical reaction between gas and oil
- No natural convection
- Swelling is negligible
- Gas diffusion is unidirectional
- The diffusion coefficient is constant
- Gas compressibility factor is constant
- Solution density remains constant

Given the cell structure shown in Figure 2-22, and the aforementioned hypothesis, diffusion was modeled as:

Fick's second law:

$$\frac{\partial^2 C_g}{\partial z^2} = \frac{1}{D}\frac{\partial C_g}{\partial t} \tag{34}$$

Initial condition:

$$C_g(z, t = 0) = 0 \tag{35}$$

The boundary condition at the bottom:

$$\frac{\partial C_g}{\partial z}\Big|_{z=h} = 0 \tag{36}$$

The boundary condition at the interface:

$$-D\frac{\partial C_g}{\partial z} = k\,[C_{g-int}(t) - C_g(z = 0, t)] \tag{31}$$

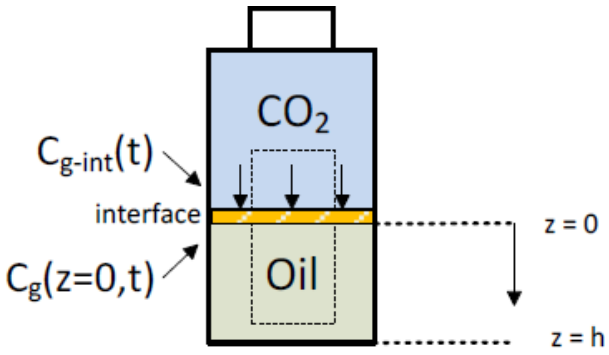

Figure 2-22. Diffusion cell

The boundary condition at the interface represents the non-instantaneous thermodynamic equilibrium. Since the gas concentration in the vapor pressure equilibrium ($C_{g-int}(t)$) does not coincide with the concentration below the interface ($C_g(z = 0, t)$), mass transfer resistance is described by the coefficient of film mass transfer resistance (1/k).

The concentration of gas above the interface in equilibrium is described by Henry's law:

$$C_{g-int}(t) = \frac{P(t)}{H} \tag{37}$$

As a further step, Equation (31), which represents the boundary condition at interface, is altered into Equation (38) in order to be implemented in the next diffusion equation solution [62].

$$\frac{\partial C_g}{\partial z} = M\frac{\partial C_g}{\partial t} - N\left[\frac{\partial^2 C_g}{\partial t\ \partial z}\right] \tag{38}$$

Where M and N are identified as:

$$M = \frac{V_{gc}M_w H}{AZRTD} \tag{39}$$

$$N = \frac{V_{gc}M_w H}{AZRTk} \tag{40}$$

The solution of the diffusion equation in the Laplace domain can be achieved by correlating the rate of mass transfer from the gas cap to the pressure decay with the rate of gas dissolution into the oil system:

$$\bar{C}_g(z,s) = \frac{MP_i[e^{((z-2h)\sqrt{s/D})} + e^{(-z\sqrt{s/D})}}{H\left[(Ms + (1+Ns)\sqrt{s/D}) + e^{(-2h\sqrt{s/D})}(Ms - (1+Ns)\sqrt{s/D})\right]} \tag{41}$$

Furthermore, the pressure-calculated equation can also be achieved in Laplace space by using Henry's law constant to substitute concentration with pressure [62]:

$$\bar{P}_{computed}(s) = \frac{MP_i\left[(e^{(-2h\sqrt{s/D})} + 1) - \frac{D}{K}(\sqrt{s/D}\, e^{(-2h\sqrt{s/D})} - \sqrt{s/D})\right]}{[(Ms + (1+Ns)\sqrt{s/D}) + e^{(-2h\sqrt{s/D})}(Ms - (1+Ns)\sqrt{s/D})]} \tag{42}$$

By using numerical methods, such as the Stehfest algorithm, to invert the Laplace transform, the variance of pressure with time can be determined with Equation

(42). The obtained results are the theoretical values represented by the diffusion model. The results are affected by the following parameters:

- Mass transfer coefficient (k)
- Henry constant (H)
- Diffusion coefficient (D)

The best values of parameters were obtained by using an objective function:

$$\text{Squared Error} = \sum_{i-1}^{n} \left(P_{exp}(t) - P_{computed}(t)\right)^2 \quad (43)$$

The purpose of this method was to determine the aforementioned three unknowns: mass transfer coefficient (k), Henry constant (H) and diffusion coefficient (D).

2.6.2.3 CT model

The use of Equation (33) is required only in the case of diffusion of liquid solvents into the oil. This will be the case of the dissolution of CO_2 in a liquid state into a light oil system. Henceforth, a change in concentration is obtained along the length of the oil column. This can be done by employing CT scan images obtained at an interval during the diffusion process. A region of interest (ROI) is allocated inside the CT scan near the liquid-oil interface and the mean of horizontal CT numbers creates a vertical profile reflecting changes in CT numbers throughout the ROI at X-ray image (See Figure 2-23).

The three required parameters can be acquired by employing the same model as defined for the pressure decay method and applying Equation (41). In order to use the concentration values obtained from Equation (33), Equation (41) was converted into a dimensionless form, since the concentration profile behavior will be plotted for a selected position below the interface. The position was fixed, and only time varied for this study.

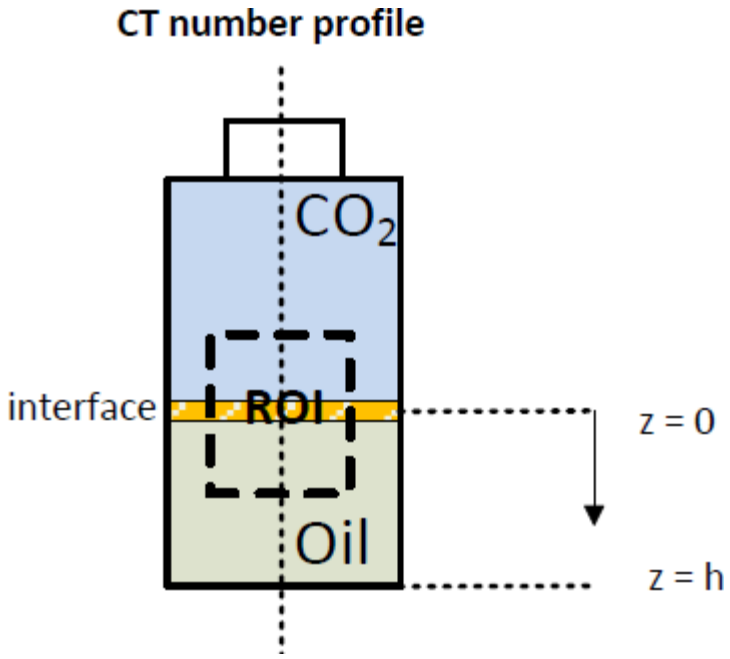

Figure 2-23. Diffusion cell ROI for CT scan

2.6.2.4 Pressure-decay and CT experiments

The pressure cells, used in the CT scanner, have the cylindrical shape to minimize CT reconstruction errors and are suitable for high-pressure levels. They are made from x-ray transparent material such as aluminum.

The monitoring of the diffusion process was accomplished by using both pressure transducer and Siemens Spirit CT scanner. As the gas diffuses and dissolves in the oil column until the system reaches equilibrium, the pressure drop is observed inside the cell. The pressure decay technique registers the pressure drop at a constant temperature.

The X-ray tomography techniques have been used to produce 2D depictions of the CO_2-oil mixture.

During the diffusion of CO_2 into oil, the concentration gradient distribution with distance can be obtained as the CT number varies throughout the process and associates to CO_2 in the mixture.

In an apparatus assembled in accordance with the configuration depicted in Figure 2-24, tests were performed.

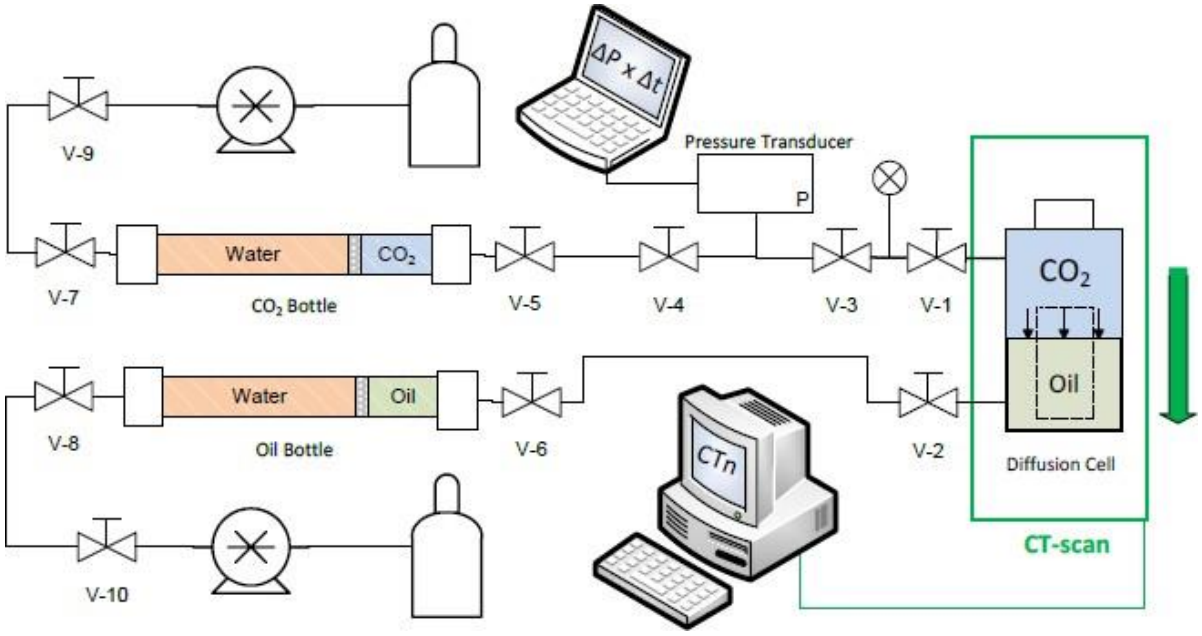

Figure 2-24. Experimental Setup

As shown in Figure 2-24, a diffusion cell with a volume of 0.00013 m^3 was connected to two pressure bottles with a fluid supply: at the top and bottom. The tests were conducted at 293.15 K in 2.76, 5.31, 9.65 and 28.96 MPa. CO_2 is lighter than oil at the first three pressure levels. Consequently, after pumping oil through the bottom, it was injected through the top and pressure is measured in the upper cell connection. In the case of 28.96 MPa, CO_2 is lighter than oil. It should be noted that for this pressure level, the gas injection was first performed which was followed with oil injection through the top. As a consequence, pressure control was carried out in the lower cell connection. The oil used during the experiment was doped with iododecane (4% in volume) to allow CT attenuation values, which detect the dissolution of CO_2 in the oil.

2.6.2.5 Results and Discussion

The data in Table 2-4 shows that both the equilibrium pressure and the equilibrium time were not significantly affected by the addition of dopant to the oil. Nevertheless, swelling may occur, taking into account density changes after the addition of dopant. Hereby, when the pressure rises from 2.76 MPa to 9.65 MPa, it takes more time to achieve equilibrium and the sharp rise of swelling can be observed from 2.76 MPa to 5.31MPa. Even at 9.65 MPa, when CO_2 is already in the liquid phase at a temperature of 293.15 K, an increase in swelling was not observed in the same portion as in the case of the first pressure variation. For the experiment with a pressure of 28.96 MPa, the oil swelling was not observed and equilibrium time was achieved faster compared to other pressures. This is most likely due to miscibility, which may have already been achieved in this condition.

Table 2-4. Experimental data obtained

Oil Types	Initial Pressure (MPa)	Equilibrium Pressure (MPa)	Equilibrium Time (hours)	Swelling (% vol.)
Normal Oil (ρ = 876 kg/m3)	5.31	3.63	37	15.7
Doped Oil (ρ = 893 kg/m3)	2.76	1.75	25	3.5
	5.31	3.86	31	12.5
	9.65	7.19	35	17
	28.96	27.85	22	N/C

Table 2-5 provides measured parameters that are best suited to the Etminan model [62] with experimental data.

Albeit the experimental conditions were never tested before in the literature, the acquired diffusion coefficients obtained from this study have the same order of magnitude of those presented in Table 2-6 and similar to those in previous studies

[49], [63] in which also the lighter components have been used than heavy oil. The Etminan model [62] can be well developed, according to experiments for both first pressures in Table 2-5 (2.76 MPa and 5.31 MPa), since these pressures fall within the same range as the Etminan analysis [62]. As a consequence, they are still at VLE and Henry law can be applied.

The investigation of diffusivity for liquid-liquid diffusion (9.65 MPa and 28.96 MPa) can still be accomplished, notwithstanding that there are many constraints in its adjustment to Etminan model [62]. As it can be noticed, the diffusion coefficient decreases during pressure change from 5.31 MPa to 9.65 MPa. The diffusion coefficient has the lowest value in the pressure decay test of 28.96 MPa. This can be explained by the fact that CO_2 was heavier than oil, and the direction of mass transfer was opposite to gravity.

As for the mass transfer coefficient, its value increases with increasing pressure. The increase in the mass transfer coefficient leads to a decrease in the film mass transfer resistance coefficient (1/k). The difference in mass transfer between VLE and LLE is proverbial. At 28.96 MPa the miscibility pressure may have already been reached. As a consequence, the larger value of the mass transfer coefficient can be observed.

Henry's constant is inversely proportional to the equilibrium concentration at a given pressure, as described by equation (37). Hence, solubility decreases for higher values of Henry’s law constant, and the predicted decay of gas cap pressure is shortened as can be seen from the first two values in Table 2-5. The Henry constant for the last two values, on the other hand, cannot be judged because of LLE.

Table 2-5. Estimated parameters for present case using pressure decay model

Pressure (MPa)	Temperature (K)	Diffusion coefficient (m^2/s)	Mass Transfer Coefficient (m/s)	Henry constant ($MPa/(kg/m^3)$)	Squared Error
2.76	293.15	$6.21x10^{-8}$	$7.33\ x10^{-6}$	$5.13\ x10^{-2}$	$2.7\ x10^{-3}$
5.31	293.15	$6.48\ x10^{-8}$	$1.02\ x10^{-5}$	$6.7\ x10^{-2}$	$4.66\ x10^{-2}$
9.65	293.15	$5.76\ x10^{-8}$	$9.00\ x10^{-4}$	$2.18\ x10^{-2}$	$2.82\ x10^{-1}$
28.96	293.15	$2.91\ x10^{-8}$	$9.98\ x10^{-4}$	$3.64\ x10^{-1}$	$6.85\ x10^{-2}$

Table 2-6. Estimated parameters in Etminan analysis used for comparison purpose.

Works	Pressure (MPa)	Temperature (K)	Diffusion coefficient (m^2/s)	Mass Transfer Coefficient (m/s)	Henry constant ($MPa/(kg/m^3)$)
Riazi, 1996	10.2	310.95	$1.12\ x10^{-8}$	$9.2\ x10^{-6}$	0.1097
Haugen and Firoozabadi, 2009	10.2	310.95	$1.30\ x10^{-8}$	-	-
Ghaderi et al., 2011	8	348.15	$1.00\ x10^{-9}$	-	10
Guo et al., 2009	20	333.15	$1.87x10^{-11}$	-	-
Etminan et al., 2013	4	348.15	$5.00\ x10^{-10}$	$1.50\ x10^{-6}$	0.11

Concerning CT model, if the data obtained using the pressure decay method in Table 2-5 is compared with Table 2-7, many discrepancies can be noticed. The squared error in the CT model is mean, with many deviations in the experimental data from the model.

One of the reasons for the differences between the models is that the former is modeled taking into account the whole system whereas the latter one is developed considering the variance of concentration in a single position chosen in z-axis over the oil column. Moreover, as was stated by Poling: "the principal experimental difficulty is that the density of a near-critical fluid is so extremely sensitive to variation in P, T, that maintaining homogeneous and stable conditions takes extreme care" [64]. Thereby, once CT model analysis is straightly concerned with the variation of density in a small portion of oil volume, minor temperature changes a priori triggers significant CT number oscillations.

Table 2-7. Estimated parameters for present case using Etminan model for CT

Pressure (MPa)	Temperature (K)	Diffusion coefficient (m^2/s)	Mass Transfer Coefficient (m/s)	Henry constant ($MPa/(kg/m^3)$)	Squared Error
9.65	293.15	9.37×10^{-6}	2.75×10^{-5}	7.27×10^{-2}	5.89×10^{-3}
28.96	293.15	2.47×10^{-9}	8.37×10^{-8}	5.5×10^{-2}	1.46×10^{-3}

2.6.2.6 Conclusion

During this study Etminan's pressure decay method [62] has proven to be a reliable technique, even for the light oil – CO_2 mixture examined. During this method, a variety of pressures were used to measure CO_2-light oil system diffusion coefficients. On the other hand, due to model limitations regarding the dissolution of gaseous solvents in oil systems, the CT scan model could only consider CO_2 in its liquid state. Despite its mean squared error, the model CT needs far more improvements than the method of pressure decay, starting with the sensitivity of CT number to the variation of the density.

2.6.3 NMR Method

In recent years, non-intrusive detection methods such as X-ray computer-assisted tomography (CAT) and magnetic resonance imaging (MRI) have been expanded to the area of diffusion investigation [65]. Nuclear Magnetic Resonance (NMR) provides advantages for self-diffusion coefficients calculation when porous media microscopic data can be acquired. The NMR pulsed-field gradient (PFG) method is non-invasive and is required to determine the diffusion coefficient [66]. Li[67] achieved the apparent diffusion coefficient mapping of oil and water by the use of NMR in porous media. The analysis of H_2O diffusion in D_2O-saturated porous media in which Fick's second law is combined with NMR was carried out by Muir [68] and Marica [69].

The purpose of this study is to determine the viability of a quantitative analysis of CO_2 diffusion and mass transfer processes in porous media utilizing MRI and to analyze the influence of various experimental conditions on diffusion coefficients.

2.6.3.1 Experimental measurements

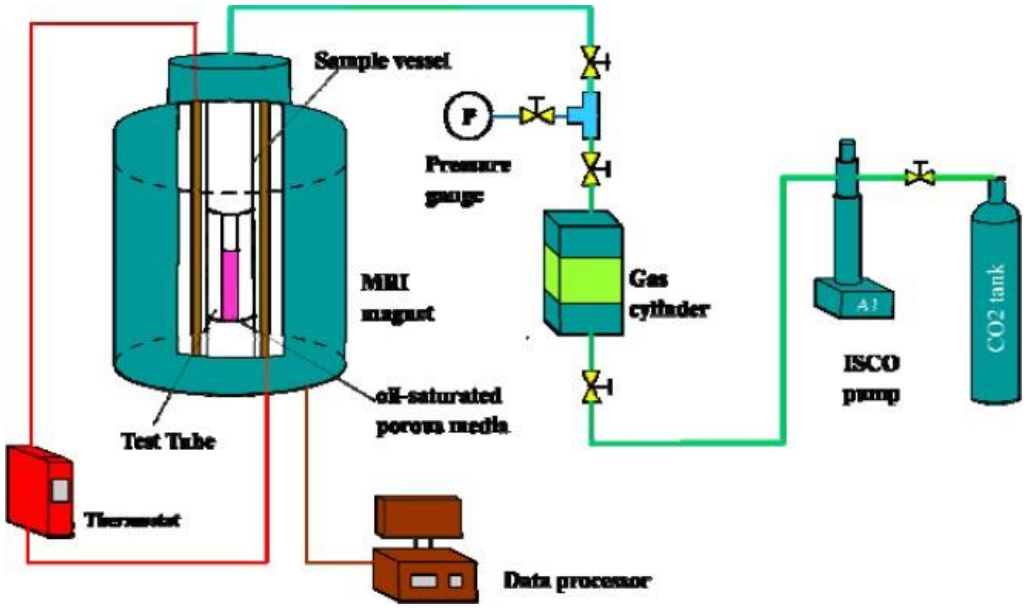

Figure 2-25. Schematic of the experimental apparent for the diffusion coefficient measurement

Figure 2-25 shows a schematic diagram of an experimental setup. The gas cylinder is a stainless steel cylinder of constant volume (500-mL) that is wrapped with an electric heater. In order to hold the diffusion samples, the MRI sample vessel is constructed of polyimide. In the tests, the outlet was blocked. The experimental vessel is separated into two parts. The inner tube has high-pressure resistance and is used for holding the sample. The outer tube provides space for liquid circulation. The temperature of the sample vessel was controlled by an inert fluid, Fluorinert™ FC-40 since it does not contain hydrogen atoms. The sample temperature in the vessel is regulated by a circulator with temperature ranges of -45 to 200 ° C and a precision of ±0.5 ° C. The specimen has a height of 10 cm and a diameter of 1 cm. A dual-chamber system was formed by the gas cylinder and the sample vessel, which can enhance the pressure stability and measurement precision when compared with a single-chamber device. In this study, CO_2 with a purity of 99.99% was used in a gaseous state and temperatures of 20°C and 30°C were selected. In this study, CO_2 with a purity of 99.99% was used in a gaseous state and temperatures of 20°C and 30°C were selected.

2.6.3.2 Mathematical analysis

From the model of a semi-infinite medium [70], the diffusion coefficients were determined as follows:

$$\frac{C_y - C_0}{C_1 - C_0} = \mathrm{erfc}\left(\frac{y}{2\sqrt{D_p t}}\right) \qquad (44)$$

Where,

- C_y - the gas concentration at distance y from the influx boundary
- C_0 - the gas concentration at the influx boundary
- C_1 - the initial gas concentration in the porous media
- erfc - the error function
- D_p - the overall diffusion coefficient
- t - time

The images produced by NMR reveal:

- The information about the oil-phase concentration
- The signal intensity of oil-phase declines
- The range of change is low

In view of the diffusion coefficient fluctuations measured by each position and each time, at the distance y, oil concentration of early time t_1 subtracts oil concentration of latter time t_2 using Equation (44), the following formula can be derived:

$$C_y(t_1) - C_y(t_2) = K\left(\operatorname{erfc}\left(\frac{y}{2\sqrt{D_p t_2}}\right) - \operatorname{erfc}\left(\frac{y}{2\sqrt{D_p t_1}}\right)\right) \qquad (45)$$

Where,

- K - the constant

Equation (45) has the advantage of ignoring the influence of the concentration change near the interface, and in a differential-profile approach, the constant impact is eliminated by subtraction.

2.6.3.3 Results and discussions

t_1 has been set for 24 min. Taking into account that the time required for the diffusion of CO_2 to the bottom of the porous media was about 192 min, t_2 was set for 48 min, 96 min, 144 min, 192 min.

Figure 2-26 depicts the corresponding result of the CO_2 diffusion in porous media at 4 MPa in 192 minutes. The initial growth trend, which is shown in Figure 2-26, was observed on each curve due to CO_2 diffusion. The downward trend of the curve arose later with the restriction of the diffusion depth.

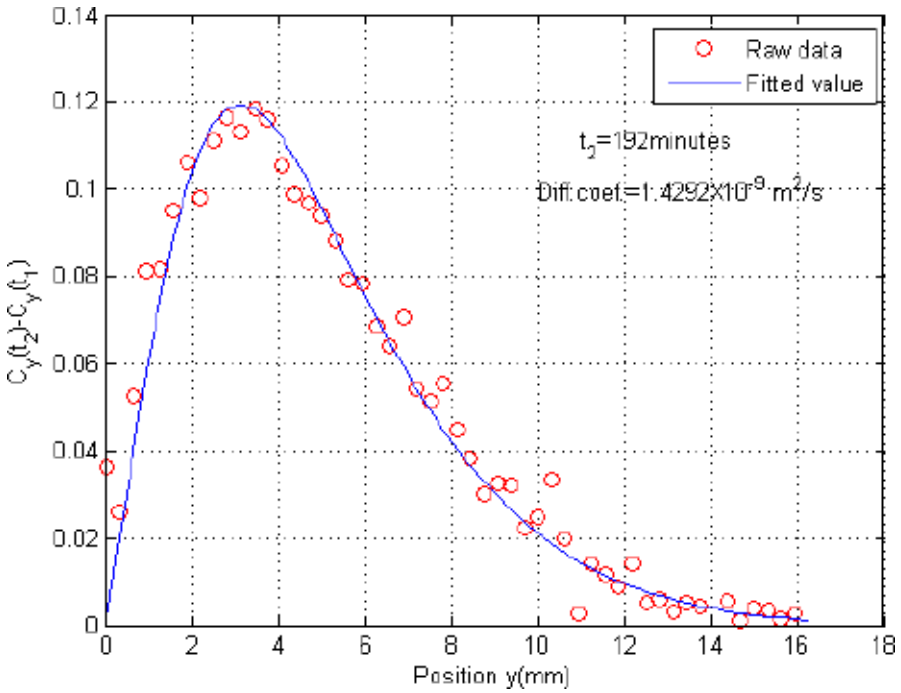

Figure 2-26. Diffusion process of CO_2 into porous media in 4Mpa of 192min

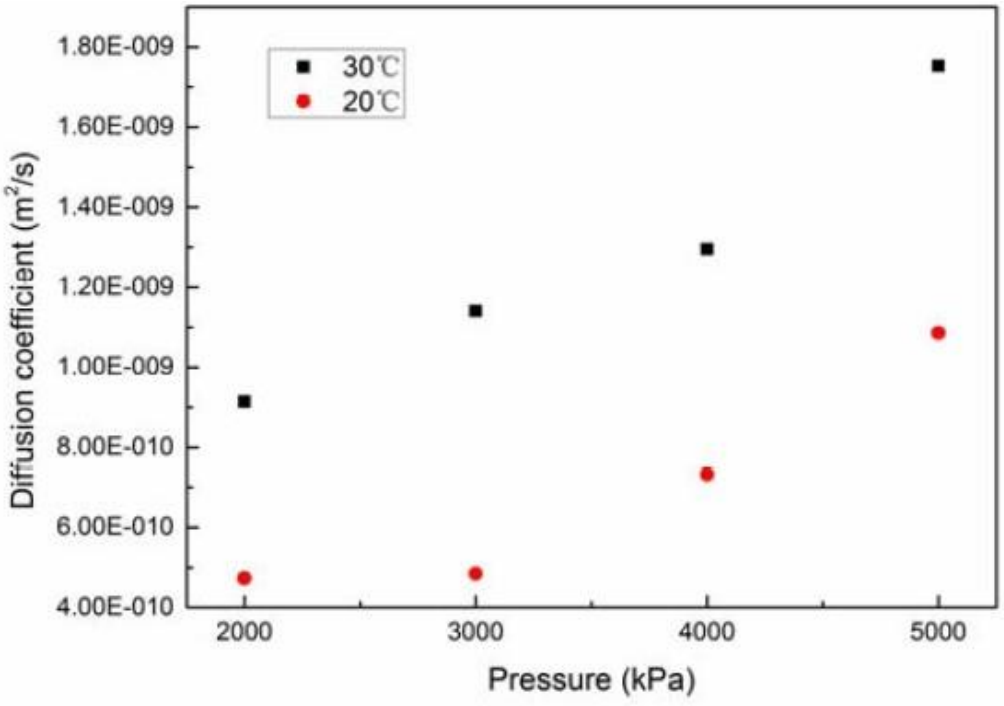

Figure 2-27. Comparison of CO_2 diffusion coefficient at different initial pressure and temperature

Using Equation (45), fitting data from four different times in one condition can achieve the best match of the diffusion coefficient The value of the effective diffusion coefficient can be calculated by averaging the four diffusion coefficients. Summary of CO_2 diffusion coefficients measured at various initial pressure and temperature is depicted in Figure 2-27.

As illustrated in Figure 2-27, the effective diffusion coefficient increases as initial pressure increases. The measured values of the effective diffusion coefficient of CO_2 varied from 0.47×10^{-9} to 1.09×10^{-9} m^2/s at 20°C, while at 30°C its value was in the range of 0.91×10^{-9} to 1.75×10^{-9} m^2/s. It should be noted that at low pressure, the increase in the effective diffusion coefficient was small while at the high pressure, the increase was high. It can be summarized that the relationship between pressure and the effective diffusion coefficient is not linear.

Regarding temperature, one can easily notice the difference in the measured values of the diffusion coefficients of CO_2 at different temperatures. The effective diffusion coefficient increases as temperature increases. The reason for this phenomenon is that an increase in temperature triggers an increase in the thermal motion of the molecules and the diffusion phenomenon exacerbates.

2.6.3.4 Conclusion

This study presented a non-invasive MRI method for measuring CO_2 diffusion through porous media. The non-linear fitting equation was presented and used to determine the effective diffusion coefficient. The advantage of this equation is that it ignores the effect of concentration changes near the interface.

From this study we may derive the following conclusions:

- The effective diffusion coefficient increases as the initial pressure increases
- The relationship between pressure and the effective diffusion coefficient is not linear

3 Conclusion

The main objective of this thesis is to analyze the diffusion phenomena of CO_2 for storage purposes. In this study, diffusion coefficients have been measured by applying different methodologies at different conditions. Taking into account all the methodologies the pressure decay method has attracted more attention due to its simplicity.

As a result of experiments, it has been observed that diffusion coefficient changes during the process of the pressure decline that the value becomes smaller towards the end of the experiment. The variation of effective diffusion coefficients that are acquired by using different parts of the pressure curve specifies that as time elapses, the value of effective CO_2 diffusion coefficient reduces. While pressure reduces as the experiment goes, the observation also reveals that the effective diffusion coefficient becomes greater under higher pressure.

Regarding temperature, the variation of the diffusion coefficients of CO_2 with temperature could be observed. The effective diffusion coefficient increases as temperature increases.

It should be noted that at low pressure, the increase in the effective diffusion coefficient was small while at the high pressure, the increase was high. It can be summarized that the relationship between pressure and the effective diffusion coefficient is not linear. Furthermore, it can be concluded that by using different methodologies, CO_2 diffusion coefficient measurements in laboratories show quite promising results in terms of safe storage of CO_2.

4 References

1. Farzam Javadpour. "*CO_2 Injection in Geological Formations: Determining Macroscale Coefficients from Pore Scale Processes*". Springer Science+Business Media, 4 October 2008.
2. Carbon Sequestration Leadership Forum Technical Group. "Enabling Large-scale CCS using Offshore CO_2 Utilization and Storage Infrastructure Developments." 08 November 2017
3. Shuaiwei Ding, National & Local Joint Engineering Research Center for Carbon Capture and Sequestration Technology, Northwest University and etc. "CO_2 Storage Capacity Estimation in Tertiary and Depleted Oil Reservoirs." International Petroleum Technology Conference. Beijing, China, 26-28 March 2019
4. https://www.sciencedirect.com/topics/earth-and-planetary-sciences/carbon-sequestration
5. https://www.mdpi.com/2076-3263/9/5/199/htm
6. Klotz, I.M.; Rosenberg, R.M. *Chemical Thermodynamics: Basic Theory and Methods*, 5th ed.; Wiley: New York, NY, USA, 1994
7. Skinner, L. CO_2 Blowouts: An Emerging Problem. *World Oil* 2003, 1, 224.
8. Xu, Tianfu. "*CO_2 geological sequestration*." United States: N. p., 2004. Web.
9. Rose, S.K.; Richels, R.; Blanford, G.; Rutherford, T. The Paris Agreement and next steps in limiting global warming. *Clim. Chang.* **2017**, *142*, 255–270.
10. Cook, J.; Oreskes, N.; Doran, P.T.; Anderegg, W.R.L.; Verheggen, B.; Maibach, E.W.; Carlton, J.S.; Lewandowsky, S.; Skuce, A.G.; Green, S.A.; et al. Consensus on consensus: A synthesis of consensus estimates on human-caused global warming. *Environ. Res. Lett.* **2016**, *11*, 048002.
11. Sharma, S.S. Determinants of carbon dioxide emissions: Empirical evidence from 69 countries. *Appl. Energy* **2011**, *88*, 376–382.
12. http://blogs.edf.org/climate411/2008/03/03/geo-sequestration/

13. https://reports.shell.com/sustainability-report/2018/sustainable-energy-future/managing-greenhouse-gas-emissions/carbon-capture-and-storage.html
14. IEA. *20 Years of Carbon Capture and Storage Accelerating Future Deployment*; IEA: Paris, France, 2016.
15. Godec, M.; Kuuskraa, V.; Van Leeuwen, T.; Melzer, L.S.; Wildgust, N. CO_2 Storage in Depleted Oil Fields: The Worldwide Potential for Carbon Dioxide Enhanced Oil Recovery. *Energy Procedia* **2011**, *4*, 2162–2169.
16. Ladbrook, B.; Smith, N.; Pershad, H.; Harland, K.; Slater, S.; Holloway, S.; Kirk, K. CO_2 Storage in Depleted Gas Fields. IEA Technical Report. 2009.
17. Holloway, S.; Vanderstraaten, R. The Joule-Ii Project the Underground Disposal of Carbon-Dioxide. *Energy Convers. Manag.* **1995**, *36*, 519–522.
18. Holloway, S. An overview of the Joule II project the underground disposal of carbon dioxide. *Energy Convers. Manag.* **1996**, *37*, 1149–1154.
19. Maloney, D.R.; Briceno, M. Experimental Investigation of Cooling Effects Resulting from Injecting High Pressure Liquid or Supercritical CO_2 into a Low Pressure Gas Reservoir. *Petrophysics* **2009**, *50*, 335–344.
20. https://www.energy.gov/fe/science-innovation/oil-gas-research/enhanced-oil-recovery
21. https://www.studentenergy.org/topics/enhanced-oil-recovery
22. https://www.scmdaleel.com/category/enhanced-oil-recovery-eor-summary/164
23. https://www.rigzone.com/training/insight.asp?insight_id=313&c_id=
24. https://www.glossary.oilfield.slb.com/Terms/e/enhanced_oil_recovery.aspx
25. https://www.investopedia.com/terms/e/enhanced-oil-recovery.asp
26. https://www.surtek.com/chemical-eor/chemical-enhanced-oil-recovery/
27. National Energy Technology Laboratory. "*Carbon Dioxide Enhanced Oil Recovery. Untapped Domestic Energy Supply and Long Term Carbon Storage Solution*." United States, March 2010
28. http://www.fossiltransition.org/pages/_enhanced_oil_recovery__eor_/135.php
29. https://www.scmdaleel.com/category/co2-injection/168

30. Samsudin, Y.; Darman, N.; Husain, D.; Hamdan, M.K. Enhanced Oil Recovery in Malaysia: Making It a Reality (Part II) (SPE-95931). In Proceedings of SPE International Improved Oil Recovery Conference in Asia Pacific, Kuala Lumpur, Malaysia, 5–6 December 2005.
31. https://en.wikipedia.org/wiki/Diffusion
32. http://perminc.com/resources/fundamentals-of-fluid-flow-in-porous-media/chapter-3-molecular-diffusion/
33. https://biologydictionary.net/diffusion/
34. https://chem.libretexts.org/Bookshelves/Physical_and_Theoretical_Chemistry_Textbook_Maps/Supplemental_Modules_(Physical_and_Theoretical_Chemistry)/Kinetics/Diffusion
35. https://en.wikipedia.org/wiki/Arrhenius_equation
36. https://en.wikipedia.org/wiki/Einstein_relation_(kinetic_theory)
37. http://perminc.com/resources/fundamentals-of-fluid-flow-in-porous-media/chapter-3-molecular-diffusion/diffusion-coefficient/importance-petroleum-engineering/
38. http://perminc.com/resources/fundamentals-of-fluid-flow-in-porous-media/chapter-3-molecular-diffusion/diffusion-coefficient/diffusion-coefficient-function-concentration/
39. https://en.wikipedia.org/wiki/Maxwell%E2%80%93Stefan_diffusion
40. https://www.comsol.ru/multiphysics/diffusion-equation
41. https://teachmephysiology.com/respiratory-system/gas-exchange/gas-exchange/
42. https://en.wikipedia.org/wiki/Fick%27s_laws_of_diffusion
43. https://www.sciencedirect.com/topics/engineering/ficks-law
44. https://eng.libretexts.org/Bookshelves/Materials_Science/TLP_Library_Vol._1/20%3A_Diffusion/20.4%3A_Fick's_Second_Law_of_Diffusion
45. Mohammed Farag. "*Lithium-Ion Batteries: Modelling and State of Charge Estimation*." June 2013
46. http://web.mit.edu/3.091s/www/Lecture_Notes/PDF_solutions/Notes_9.pdf
47. https://perminc.com/resources/fundamentals-of-fluid-flow-in-porous-media/chapter-3-molecular-diffusion/diffusion-coefficient/measurement-techniques/

48. https://perminc.com/resources/fundamentals-of-fluid-flow-in-porous-media/chapter-3-molecular-diffusion/diffusion-coefficient/measurement-techniques/pressure-decay-method/
49. Riazi, M.R., A new method for experimental measurement of diffusion coefficients in reservoir fluids. *J. Pet. Sci. Eng.* 14 (1996)
50. https://perminc.com/resources/fundamentals-of-fluid-flow-in-porous-media/chapter-3-molecular-diffusion/diffusion-coefficient/measurement-techniques/refractive-index-method/
51. https://perminc.com/resources/fundamentals-of-fluid-flow-in-porous-media/chapter-3-molecular-diffusion/diffusion-coefficient/measurement-techniques/nmr-method/
52. https://perminc.com/resources/fundamentals-of-fluid-flow-in-porous-media/chapter-3-molecular-diffusion/diffusion-coefficient/measurement-techniques/nmr-method/application-low-field-nmr-diffusion-measurements/
53. https://perminc.com/resources/fundamentals-of-fluid-flow-in-porous-media/chapter-3-molecular-diffusion/diffusion-coefficient/measurement-techniques/computer-assisted-tomography/
54. Bao Jia, Jyun-Syung Tsau, and Reza Barati, University of Kansas: "*Measurement of* CO_2 *Diffusion Coefficient in the Oil-Saturated Porous Media"* November 2018.
55. Li, Z., Dong, M., and Shirif, E. 2006. Transient Natural Convection Induced by Gas Diffusion in Liquid-Saturated Vertical Porous Columns. *Industrial & Engineering Chemistry Research* **45**: 3311–3319.
56. Li, Z., Dong, M. 2009. Experimental Study of Carbon Dioxide Diffusion in Oil-Saturated Porous Media under Reservoir Conditions. *Industrial & Engineering Chemistry Research* **48**: 9307–9317.
57. Ghasemi, M., Astutik, W., Alavian, S. A. et al. 2017. Determining Diffusion Coefficients for Carbon Dioxide Injection in Oil-Saturated Chalk by Use of a Constant-Volume-Diffusion Method. *SPE Journal* **22** (02): 505–520.
58. Renner, T.A. 1988. Measurement and Correlation of Diffusion Coefficients for CO_2 and Rich-Gas Applications. *SPE Reservoir Engineering* **3** (02): 517–523.

59. Gamadi, T.D., Sheng, J.J., Soliman, M.Y., et al. 2014. An Experimental Study of Cyclic CO_2 Injection to Improve Shale Oil Recovery. SPE Improved Oil Recovery Symposium, Tulsa, Oklahoma, USA. SPE 169142.
60. GEM. 2016. GEM USER GUIDE: Compositional & Unconventional Reservoir Simulator. Computer Modelling Group Ltd.
61. S.V. Araujo, J.A.V. Vargas, O.V. Trevisan, State University of Campinas, R.G. Santos, University Center of FEI, *Diffusion Coefficient of CO_2 in Light Oil Under Reservoir Conditions Using X-Ray Computed Tomography*, Offshore Technology Conference, Rio de Janeiro, Brazil, 29–31 October 2013.
62. Etminan, S. R., Pooladi-Darvish, M., Maini, B.B., et al. 2013. Modeling the interface resistance in low soluble gaseous solvents-heavy oil systems. Fuel 105 672-687. http://dx.doi.org/10.1016/j.fuel.2012.08.048.
63. Haugen, K. B. and Firoozabadi, A. 2009. Mixing of two binary nonequilibrium phases in one dimension. AIChE Journal 55 (8) 1930–1936. http://dx.doi.org/10.1002/aic.11814.
64. Poling, B. E., Prausnitz, J.M. and O'Connell, J.P. 2001. The properties of gases and liquids. New York City: McGraw-Hill Book Company.
65. Junlin Chen, Yuechao Zhao, Yongchen Song, Di Wu, Dayong Wang, *Experimental Measurement of CO_2 Diffusion Coefficient in Porous Media using NMR Micro-Imaging,* International Symposium on Energy Science and Chemical Engineering (ISESCE), 2015
66. E.L. Cussler, Diffusion: mass transfer in fluid systems, Cambridge university press, 2009.
67. L. Li, F. Marica, Q. Chen, B. MacMillan, B.J. Balcom, Journal of Magnetic Resonance, 186 (2007) 282-292.
68. C. Muir, B. Lowry, B. Balcom, New Journal of Physics, 13 (2011) 015005.
69. F. Marica, S.A.B. Jofré, K.U. Mayer, B.J. Balcom, T.A. Al, Journal of contaminant hydrology, 125 (2011) 47-56.
70. J. Crank, The mathematics of diffusion, Oxford university press, 1979.